

IN VIVO RAMAN SPECTROSCOPIC ANALYSIS OF HSP70 AND LASER
PRECONDITIONING IN MURINE INCISIONAL WOUNDS

By

Alexander James Makowski

Thesis

Submitted to the Faculty of the
Graduate School of Vanderbilt University
in partial fulfillment of the requirements
for the degree of

MASTER OF SCIENCE

in

Biomedical Engineering

May, 2010

Nashville, Tennessee

Approved:

Professor E. Duco Jansen

Professor Anita Mahadevan-Jansen

ACKNOWLEDGEMENTS

Firstly, I would like to thank my fiancée Johanna, my love, my inspiration and my drive, the basis of my motivation and organization, without whom none of this would have been possible. I would also like to thank my parents who have always supported all of my endeavors with more love and patience than should be humanly possible. My brother Evan is always there when I need someone to talk to. My best friend Patrick puts up with all of my nonsense and never fails to make me smile.

I feel blessed to have met my advisors and mentors. I am truly happy to call them both colleagues and friends. Though he will be taken aback to hear it, Duco Jansen is both crazy and brilliant in the way that makes everyone around him want to get up in the morning to do science. Anita Mahadevan-Jansen has known me for years, and it shows. She keeps me focused while pushing me ever forward. Jeff Davidson has the utmost patience with me, and always manages to find the perfect words to reassure me when I am lost. I also want to thank Jerry Wilmink, Josh Beckham, and Alex Abraham. Aside from laying the groundwork that made this thesis possible scientifically, they each invested countless hours training me, instructing me, and happily answering endless late-night and early morning phone calls.

I would like to acknowledge the financial support that made the completion of this work possible. A research grant from the American Society for Laser Surgery and Medicine provided funding for the equipment and resources necessary to investigate the biochemical effects of laser preconditioning on subsequent healing wounds. Without the facilities and expertise of the Medical Free Electron Laser center (AFOSR F49620-01-1-0429), this work would not have been possible. The Contag Lab at Stanford University graciously donated transgenic hsp70-luc mouse models for the investigation of the role of hsp70 in this process. Raman equipment used in this study was funded through the National Institute of Health.

TABLE OF CONTENTS

ACKNOWLEDGEMENTS	ii
LIST OF FIGURES	iv
I. INTRODUCTION	1
Overview of Wound Healing	1
Normal Wound Healing	2
Impaired Wound Healing	9
Diabetic Foot Ulcers: Prevalence, Complications, and Possible Causes	9
Chemical and Thermal Burns	12
Animal Models of Wound Repair and Analysis Measures	13
Enhanced Wound Healing	18
Lasers for Wound Healing Enhancement	18
Heat Shock Proteins in Wound Healing	20
Optical Analysis of Wound Healing: Raman Spectroscopy	23
Summary	29
II. IN VIVO ANALYSIS OF LASER PRECONDITIONING IN INCISIONAL WOUND HEALING OF WILD-TYPE AND HSP70 KNOCKOUT MICE WITH RAMAN SPECTROSCOPY	35
Abstract:	35
1. Introduction:	36
2. Methods:	40
2.1 Mouse Model and Preparation:	40
2.2 Laser Preconditioning and Surgery:	42
2.3 Raman Spectroscopy: Acquisition and Processing:	43
2.4 Histology:	44
3. Results:	45
3.1 Establishing normal tissue spectral behavior:	45
3.2 Spectral content of preconditioned wounds and effects of HSP70:	49
3.3 Peak ratios elucidate the combined effects of HSP70 and preconditioning:	53
3.4 Histology confirms collagen organization:	57
4. Discussion:	60
4.1 Characterizing normal incisional wound healing	60
4.2 Spectral content implies HSP70 role in wound healing and laser preconditioning:	62
4.3 Mouse model and experimental limitations:	63
4.4 Significance of peak ratios through the wound healing time course:	64
4.5 Histology confirms RS trends for HSP70 and laser preconditioning	66
4. Conclusions and Future Directions:	67
Works Cited	69
III. FUTURE DIRECTIONS	71

LIST OF FIGURES

I.1	Wound Healing Diagram (P. Martin, 1997).....	5
I.2	Collagen Formation (Alberts et al., 2002).....	8
I.3	HSP70 Biochemical Pathways (Beere et al. 2005, Morimoto et al.,1996).....	21
I.4	Jablonski Diagram (Iari-Gabriel Marion, 2010).....	24
II.1	Mouse Model Experimental Diagram.....	8
II.2	Wild Type Wound Healing Time Course.....	13
II.3	Peak Intensity Differences of Mean Spectra Relative to Pre-Op (POD2, POD7).....	15
II.4	Comparison of Average Wild-Type and HSP70 Knockout Wound Spectra on POD2....	17
II.5	Comparison of Average Preconditioned and Untreated Wound Spectra on POD2.....	19
II.6	Paired Comparisons of Time Course Average Peak Ratio Intensity of 1440:1657cm ⁻¹ in lateral wound samples.....	21
II.7	Paired Comparisons of Time Course Average Peak Ratio Intensity of 1304:1265cm ⁻¹ in lateral wound samples.....	23
II.8	Polarized microscopy of H&E stained wound cross-sections at POD4	25
II.9	Polarized microscopy of H&E stained wound cross-sections at POD7	26

CHAPTER I

INTRODUCTION

Overview of Wound Healing

Wound healing is a coordinated succession of concurrent biochemical and cellular events that result in the restoration of tissue architecture and function [1]. Within the context of normal physiology, these processes follow a specific and well-characterized time course. Aging and chronic disorders, including diabetes, create pathologies that impair the normal sequence of wound healing [2] causing many patients to eventually develop chronic foot ulcers [4-6]. Complex wound conditions including thermal and chemical burns result in structures that naturally impede the mechanisms of normal wound healing, retarding the time course and increasing risk of infection. Wound healing disorders represent a significant health care issue in both cost and morbidity, affecting patient quality of life through decreased functional integrity of the skin as an organ and frequent limb amputations. An annual cost to the US Health Services in excess of \$9 billion for age-related wound impairment, underscores the drastic adverse impact of impaired wound healing on quality of life through decreased mobility, decreased independence, and suffering under chronic pain [7].

While modern pathology and molecular biology methods have excelled at determining normal wound healing mechanisms, application of this knowledge to impaired wound healing states have yielded mixed results. Unacceptable mortality rates and a growing number of limb amputations, roughly 100,000 per year in the US alone from diabetic foot ulcers, have sparked investigation into a variety of novel preventative and treatment strategies for enhancement of wound healing. There is a specific need for a non-invasive technology capable of enhancing impaired wound healing through intrinsic mechanisms. The plethora of nascent therapeutic

modalities attempting to meet this demand has also given rise to a specific need for detection of structural and functional changes within the healing wound to better understand the mechanisms of impairment and evaluate treatment response. Ideally, such a technology would readily allow for translation of results from laboratory studies to clinical use.

Normal Wound Healing

To fully understand the complex and balanced process of dermal wound healing, it is best framed in the context of the precise composition and overall function of the skin. Paul Martin conducts an excellent review of the biological processes involved in dermal wound healing, as a function of skin physiology, disease states, and efforts towards "perfect regeneration". Skin is composed of a "keratinized stratified epidermis" above a connective tissue matrix, composed largely of collagen fibers. The primary function of skin is to serve as a protective barrier against the outside world. When this barrier is violated by the creation of a wound, a clot is formed to prevent infection and blood loss. The remainder of the wound healing process is an attempt by the body to then replace this clot with new skin while still preserving skin function. In a complex organizational scheme, each cellular and structural component plays multiple roles to ward infection and reestablish structure, starting with the clot. Clots are composed primarily activated platelets that cause the cross-linking of fibrin, together forming the structure of the clot. During clot formation, the degranulation process of these platelets releases a massive biological signal composed of growth factors and cytokines. This triggers all four of the major components of early wound repair: the recruitment of inflammatory cells, reepithelialization, wound contraction, and wound angiogenesis. [3]

Though considered the first major step in wound healing, the recruitment of inflammatory cells is crucial to the continued process of wound healing. It happens along a well-characterized time course, and its malfunction is often considered the source of healing

impairment in disease states. While platelets do send an essential signal to circulating leukocytes involved in the inflammation response, it has been shown that peptides from digested bacteria and byproducts of matrix proteolysis also generate important chemotactic gradients that attract these crucial cells. Before these immune cells can participate in the wound healing process, they first must exit the circulation through the processes of diapedesis and extravasation. Through cellular signaling via integrins and selectins, these leukocytes roll along vessel walls, adhere to specific sites, and then force their way through the vascular epithelium. This process is of special interest because its malfunction is newly attributed to numerous chronic disease states, including impaired diabetic wound healing [8, 9].

Martin explains that within the time course of inflammation, the neutrophils arrive first to combat the pathogens due to the wound. Barring serious infection, these neutrophils eventually degrade, but not before releasing cytokines to signal to other leukocyte types. After a few days, macrophages predominate the wound environment. Macrophages are primarily phagocytic in function, digesting foreign bodies, spent neutrophils, cellular debris and matrix byproducts; however, macrophages release growth factors that effectively amplify the original signal generated by the clot. [3]

Reepithelialization is defined as the cumulative actions by which remaining epithelial cells (specifically keratinocytes) reform the outermost layers of the skin. This process lags behind inflammation for several reasons. In normal skin, the lowest layer of epithelials, the basal keratinocytes, are anchored by hemidesmosomes to the special layer of matrix called the basal lamina. Before these cells can reform continuous layer destroyed by the wound, they must first digest the current hemidesmosomes, alter their expression of integrins, and arrange actin fibers for locomotion. This process also has a level of elegance and complexity that is still being investigated. Martins reports that more recent studies imply the activity of suprabasal (above the basal cells) keratinocytes in locomotion and reestablishing the epithelial layer. Moreover, it has

been found that intact cells from remnants of gland or follicle structures also undergo cellular changes and act as a locomotive healing front. Beyond locomotion, differentiation, and mitosis, these cellular layers must also cut a path through the fibrin clot by expression of matrix metalloproteinases (MMPs) and via activation of local plasminogen (within the clot) to yield plasmin, one of the few enzymes capable of degrading fibrin. Once the keratinocyte layer is fully established, the cells cease to migrate, begin to express "normal" integrins, and reattach to the basal lamina. Ongoing research focuses on the regulation of this cellular migration, as the expression of growth factors and their relative effects on the involved cells are seen as potential targets to modulate wound healing (discussed below). [3]

Concurrent with, but lagging even further behind reepithelialization is the overall contraction of the wound site. Initial contraction is a physical response, as cellular contractile fibers assist in bringing the apposed edges of the wound closer together. The majority of the contraction process, however, occurs through the degradation and deposition of matrix proteins via dermal fibroblasts which proliferate in response to the early cytokine and growth factor signals. A 3 to 4 day lag time for this process is reported by Martin, explained by the generation of cellular machinery not normally present in the dermal fibroblast, rather than the time required for proliferation. Dermal fibroblasts respond not only to local growth factors and cytokine signals, but also to the proteins they contact. Ultimately, they are responsible for the digestion of the fibrin clot and deposition of the replacement matrix. [3, 8]

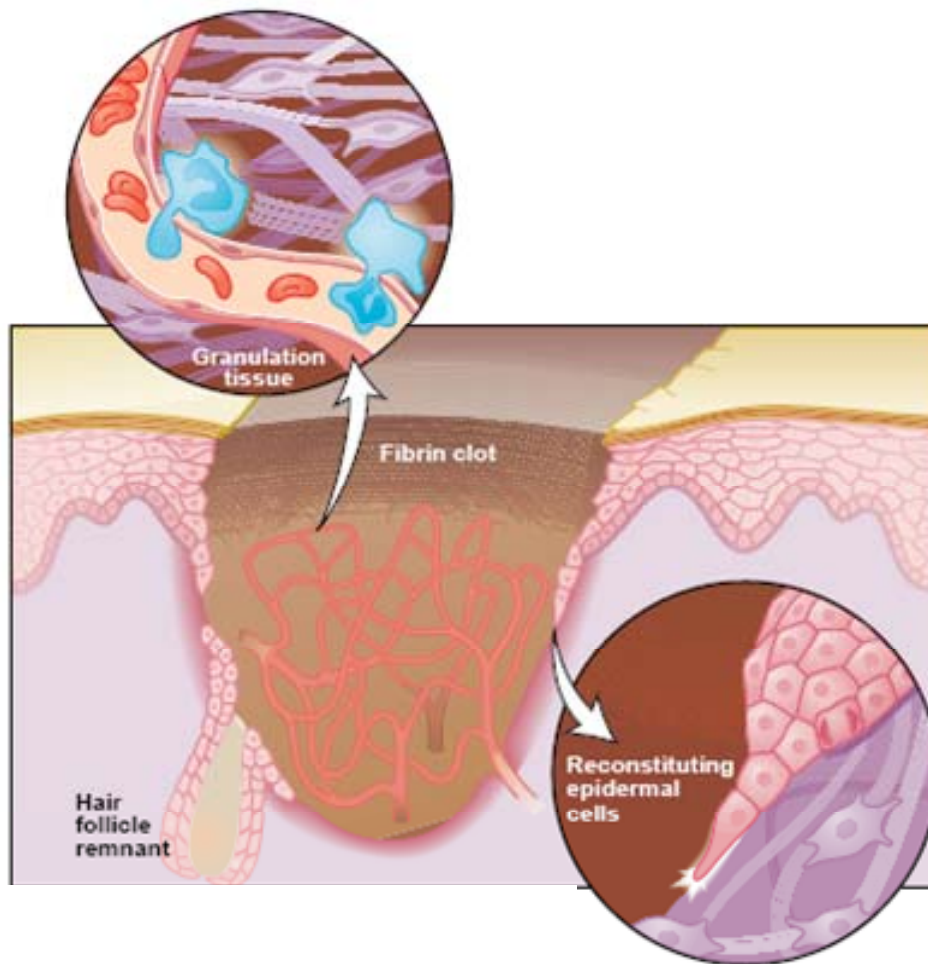


Figure 1. Cartoon illustrates inflammatory cell infiltration, the moving reepithelialization front, and the fibrin clot capillary plexus, characteristic of early wound healing. (P. Martin 1997) [3]

Beyond the cellular and subcellular orchestration of wound healing signals, the tissue level remodeling of the healing wound also appears to be well-regulated. Growth factors associated with angiogenesis, specifically VEGF (Vascular Endothelial Growth Factor) and FGF (Fibroblast Growth Factor), are expressed by locomotive epithelial fronts to direct the growth of new blood vessels. Moreover, Martin cites studies that indicate the regeneration of hair follicles and sweat glands that are integral to greater function and maintenance of the skin as an organ. Compared to the mechanism of basic wound repair, relatively little is known about the

mechanisms behind these processes. Nevertheless, studies indicate that the regeneration of these structures has been linked to different growth factor expression that corresponds to the end of the wound healing time course. These growth factors, in particular, are associated with embryonic wound healing, which is noted for its specific lack of scarring. Beyond cosmetic issues, the lack of scarring is significant because scars do not contain the level of organization or hierarchical structure associated with normal skin. Martin concludes the review with the idea that knowing the differences between the two healing processes would provide invaluable knowledge into the modulation of intrinsic mechanisms within this highly orchestrated process to achieve better results in normal and diseased wound healing.[3]

To fully achieve a normal reconstruction of skin, the complex structure of the extracellular matrix (ECM) must be properly restored. The extracellular matrix consists of both fibrillar proteins and glycosaminoglycans, lending it tensile strength and turgor pressure, respectively. Neighboring resident cells create and exocytose these molecules to be incorporated into the surrounding matrix. In brief, the primary glycosaminoglycans are chondroitin sulfate, heparan sulfate, keratan sulfate, and hyaluronic acid. The primary fibrillar components are collagen, elastin, fibronectin, and laminin [10]. Beyond the structure that these proteins lend to the body, the matrix itself contains embedded cues and site-specific posttranslational modifications that dictate behavior and act as "guideposts" to local cells. These cues become especially important in situations where the matrix is damaged. In these instances, fragments of the broken structural proteins have also been shown to act as chemotactic signals for repair and degradation mechanisms [11]. Many of the ECM proteins are actually complex fibrillar structures assembled outside the cell from specific components in highly coordinated sequences. The creation and incorporation of these proteins into the matrix is spatially specific and is encoded by complex genetic processes [12].

While dysfunction in these mechanisms accounts for a wide array of arguably rare congenital defects including Marfan syndrome, Ehlers Danlos Syndrome, and Alport's Syndrome, knowledge of the proper function of ECM protein deposition is crucial to understanding the likely mechanisms behind chronic wound deficits [12]. As a brief example, the later stages of diabetes are associated with impaired wound healing. It is commonly believed that numerous systemic effects are responsible for this deficit, but collagen posttranslational modifications may play a role [8]. These molecules, which are mostly pendant disaccharides, are known to direct the proper incorporation of the molecule into the matrix as well as signal fibroblasts during the repair and deposition process. An increase in interstitial sugar concentration, as seen in diabetes, could lead to the polymerization of pendant disaccharides. "Masking the guidepost", these changes could affect both the proper creation of collagen fibrils and the ultimate incorporation into the matrix itself. Current theory supports that the glycosylation of these advanced glycosylated end products (AGE) onto matrix structural proteins is also responsible for the downward spiral of inflammation-mediated degradation, resulting in chronic wound persistence [8, 13].

Equally as important as the mechanisms of creation and repair are the functions of the ECM proteins, themselves. While the extracellular matrix is composed of countless proteins and glycosaminoglycans mixed in varied concentrations at specific locations, perhaps the three most important elements by structural and functional contribution in the dermis are collagens, fibronectin, and elastin.

Collagen: The term collagen is perhaps a misnomer, as it refers more to a structural domain found in a wide variety of proteins (ranging from the flexible constituent of bone, to the neurotransmitter Acetylcholine), rather than a specific protein. Fibrillar collagens, named for the long fiber structure commonly known as collagen, dominate the structural components of the ECM. Specific collagens are usually spatially localized and are specified by the combination of

tropocollagen fibers that make up their triple helical superstructure. The thermal tolerance and structural properties of collagen are due largely to hydroxyproline, a molecule almost unique to collagen within the body. Specific combinations of constituent tropocollagens determine the function and mechanical properties of the larger collagen fibril. Type I fibrillar collagen is the primary structural component of skin, yet Type III fibrillar collagen lends skin its extensible properties. Other collagens also exhibit the typical triple helical domains, but do not form larger fibrillar structures. Type IV collagen cross-links extensively to form the basal lamina of the skin. While low in concentration Type VII collagen plays a critical role in anchoring the basal lamina of the skin to underlying structures. [11]

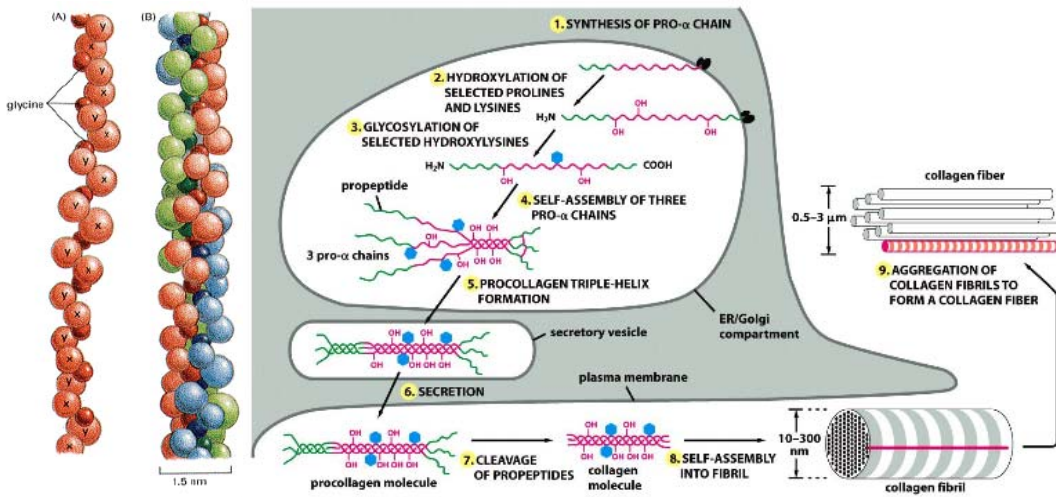


Figure 2. The structure and formation of collagen. Left shows the Gly-X-Y repeating structure (where X and Y are normally proline and hydroxyproline, respectively). Right illustrates the detailed formation of a collagen fibril relative to cellular location. (Alberts et al. 2002) [18]

Fibronectin: Fibronectin is an ECM glycoprotein known for its ability to bind integrins, collagen, fibrin, and syndecans. When incorporated into the matrix, it exists as a homodimer linked by disulfide bridges. Usually secreted by fibroblasts as a soluble dimer, it is later incorporated into the matrix directly. Significantly, this protein can link ECM structural

components directly to cells. Subsequently, fibronectins play a significant role in cell adhesion and migration. Though many forms of fibronectin exist throughout the body through alternative splicing, most are directly associated with cell adhesion to the ECM. Notable is its other soluble form, plasma fibronectin, a major constituent of blood manufactured by the liver. Upon tissue injury, plasma fibronectin is incorporated into the temporary matrix formed as a clot. Throughout the course of wound healing this clot is degraded, and subsequent fibronectin byproducts become cellular signals. Research by Valenick et al. suggests that $\alpha4\beta1$ integrin binding, crucial to cellular contraction and the proper progression of healing, is enhanced by the presence of these fibronectin fragments. [11, 14]

Elastin: Elastin is the protein in connective tissue that confers most of the deformation tolerance to skin and other connective tissues. Elastin is composed of tropoelastin monomers cross-linked at lysine residues by lysyl oxidase. Elastin is amorphous in structure when relaxed due to its mobile hydrophobic regions, but its regular repeats and cross-linked pattern become apparent upon stretching. When incorporated into connective tissues and skin, elastin is surrounded by a sheath of glycoproteins (primarily fibrillin) forming the overall structure of elastic fibers. [15]

Impaired Wound Healing

Understanding the cellular and structural elements of normal dermal wound healing allows for the investigation into situations of mechanistic failure. This review focuses on the complex situation of diabetic foot ulcers, while including a somewhat more basic biological situation of burn wounds.

Diabetic Foot Ulcers: Prevalence, Complications, and Possible Causes

The National Institute of Diabetes and Digestive and Kidney Diseases (NIDDK) reports that there were 20.8 million diabetic patients in the United States in 2005, representing 7% of the

total population and an estimated direct medical cost exceeding \$90 billion in 2002 [5]. Long-term hyperglycemia significantly impairs normal wound healing mechanisms in the diabetic population, although the underlying cellular mechanisms of this impairment are largely unknown [16]. Advanced diabetic complications (cardiovascular disease, atherosclerosis, and peripheral neuropathy leading to numbness) amplify the risk of this impaired wound healing, making diabetics increasingly vulnerable to chronic wound formation, especially diabetic foot ulcers, which are currently the most common wound care problem in the United States.

Bennett et al. conducted a comprehensive review of the underlying mechanisms of diabetic foot ulcers, relating these to development of current therapeutics [17]. The two most significant risk factors in diabetes that result in foot ulcers are peripheral neuropathy and ischemia. Through peripheral neuropathy, changes in gait lead to improper loading, while coincidental numbness prevents body's normal feedback mechanism of pain from reporting the pattern. Moreover, loss of normal sweating response leads to degradation of skin integrity and increased risk of infection over time. Through ischemia (associated with high incidence of lower limb atherosclerosis in diabetic patients), low tissue oxygenation can lead to stress and necrosis. Recalling that the normal wound healing course, inflammation and signaling is conducted through local vascular flow, one can see that ischemic conditions impede subsequent wound healing as well. [18]

Roughly 20 – 25% of the diabetic population, or 4 – 5 million patients, require treatment of foot ulcers at least once in their lifetime, making these lesions responsible for more hospitalizations than any other complication from diabetes. These wounds remain in a chronic inflammatory state while the body is unable to follow the normal wound healing response, and therefore these lesions generally have difficulty healing. Treatment of foot infections requires coordinated clinical management with attention to both local and systemic issues [19, 20]. Therapeutic strategies used today include repeated debridement, offloading, and dressings for

lower grade ulcers, and broad spectrum antibiotics and occasionally limited or complete amputation for higher grades, requiring a team effort of health care workers from various specialties [21]. Approximately 100,000 limb amputations per year are a direct result of diabetic foot ulcers while morbidity from these chronic wounds remains unacceptably high. This figure will likely continue to rise given the major public health issue that “diabesity” has become.

Citing institutions such as the American Hospital Association and reports from the US Health Services, reviews of age-related chronic wound prevalence and cost present figures in the range of \$9-20 billion annually, representing over 5 million patients [7, 22]. Discrepancies in these numbers and the relationship between chronic wounds, aging, and disease are directly addressed in such reviews as the result of inadequate definition and aspecific diagnosis of a chronic wound situation arising from a multitude of concurrent mechanisms. Moreover, these numbers are considered to be obscured by the correlation between chronic wound development and decreased mobility, leaving a significant population undergoing treatment via home care. The ill-posed definition of chronic wounds begets discrepancies in treatment and research development. Reviewing clinical cases and outcome measures, Matousek et al. explains that a recent interest in more “objective” measures is well placed but slow in progress [4]. He cites that outcome measures for therapeutic efficacy in chronic wounds remain largely uncontrolled, and that few studies attempt to correlate clinical and laboratory science findings. After declaring current gold standards for treatment therapeutics insufficient for translation between scientific and clinical application, he calls for a unification of outcome assessment.

The suboptimal clinical outcome has lead scientists to explore new strategies for limiting development of foot ulcers, such as new off-loading techniques and dressings, artificial skin grafts, growth factors, and alternate methods of debridement [23]. While the use of some of these growth factors has elicited encouraging results in animal models and controlled pilot clinical studies, many problems plague these methods in the arena of clinical use. Bennett blames much

of the mixed results in clinical trials to small trial sizes and inconsistent endpoints [17]. Nevertheless, varying treatment response rates and dosimetry, coupled with short half lives, local inactivation, and poor bioavailability through current delivery vehicles are leading researchers like Eming and Benn to research alternative transfer vehicles like particle mediated gene delivery of growth factors, specifically PDGF (platelet derived growth factor) and TGF β -1 (transforming growth factor), to increase delivery efficacy and bypass degradation [24]. Benn showed increase in wound tensile strength of both diabetic and nondiabetic rats via particle mediated gene transfer with TGF β -1 cDNA's [25]. Though also encouraging and not likely as short lived as topical applications, they are likely as expensive. Furthermore, these methods bear the limitations and risks of treatment efficiencies associated with current gene transfer methods of drug delivery. Despite these efforts, early recognition of foot ulcer symptoms and rigorous, continuous management remain the most effective strategy in the treatment of diabetic foot ulcers [26]. Thus, researchers continue to search for a local or systemic therapeutic strategy that can measurably accelerate wound healing in both early and late stages of diabetic wound formation.

Chemical and Thermal Burns

Burn wound care has become an increasing military interest. Epidemiological studies from current military operations in Iraq and Afghanistan indicate a shift to a greater percentage of morbidity due to explosion [27]. In current engagements, 81% of the wounds were a result of an explosion (improvised explosive device or IED, landmine, mortar, bomb, and grenade) as compared to 65% in Vietnam, 73% in WWII, and 35% in WWI [28]. Explosive wound types are described in the report as those resulting from pressure waves, penetrating projectiles, blunt trauma, and thermal burns. Thermal burn wounds are the most difficult to treat explosion wounds in terms of recovery time, pain, infection risk, and cosmetic appearance. The report furthers that an increase in the number of improvised explosive devices targeted to vehicles have led to a

subsequent increase in thermal burns through secondary mechanisms, including burning vehicles, clothing and equipment.

Skin exposure to severe partial thickness or full thickness thermal burns (and chemical burns) can take up to three months to heal [29]. Burn wounds necessitate constant care for full recovery. The combination of the physical and chemical changes in tissue leads to the creation of a compromised wound periphery that contains large quantity of denatured protein and poor circulation. This charred area, called eschar, is a perfect breeding ground for bacteria, and subsequent ischemic necrosis in the surrounding area requires a situation of constant physical removal (debridement) to ensure proper healing. Though technologies are being developed to assist in the treatment of burn wounds, the debridement of eschar is currently a painful mechanical process that yields best results with frequency. [30]

Animal Models of Wound Repair and Analysis Measures

Much work has been done on advancing the accuracy of animal models for human wound repair [31]. Murine models (which dominate in this area by availability of numerous genetically modified phenotypes, low cost, maintenance, reagent availability and previous research data availability), express phenotypes that are more readily applicable to acute wound repair than to chronic wounds. There is difficulty in modeling chronic wounds due to the physiologic differences between animal and human repair [31].

The type of wound inflicted on the animal model directly affects the types of measurements that can be conducted as part of the study. Advanced histological image processing and biochemical content assays like microarray are more feasible when utilizing full thickness excisional wounds (i.e. removal of a significant volume of tissue and the filling of the void). Excisional wounds are usually created with a biopsy punch, and subsequent healing rates are monitored as a function of wound volume or cross-sectional area, extent of reepithelialization, histological organization, and collagen content. However, the excision of the loosely attached

skin of rodents leads to significant wound closure by contraction, which results in rapid shrinkage of the surrounding skin in a presumably adaptive fashion due the reaction of contractile filaments. The presence of contraction reduces wound volume to an extent far greater than what is encountered in human wound healing [31]. Contraction creates a source of organism specific variation, limiting the extent of granulation tissue, leukocyte infiltration, and reepithelialization, all of which are crucial features scored in semi-quantitative histological analyses. Experimentally, contraction is readily limited by splinting of the wound with retaining rings.[31]

Incisional wounds, while easier to create and replicate than excisional wounds, have an extremely limited volume of granulation tissue for biochemical analysis as well as a significantly smaller histological cross-sectional area. However, incisional measurements offer the distinct advantage of biomechanical evaluation via tensiometry. Unlike many measures of wound healing dynamics, tensiometry provides quantitative data regarding structural elements of the healing wound. In tensiometric experiments, wounds are segmented transversely into strips of defined length and width. Using the principles of biomechanics for testing viscoelastic solids, tissue samples are test for stress and strain capabilities. Skin samples usually undergo "priming", in which they are stretched to a predefined stress or strain two to three times before they are strained to rupture. The machine records tensile load, stress, and strain, such that parameters like Young's Modulus and the maximum tensile load can then be calculated. While quantitative, tensiometry requires sample consumption, precise measurement of sample volume, and precise loading technique to yield accurate data.[31]

Burn wounds, while perhaps the most accurate physiological comparison of impairment between species, offer the greatest complexity in creation and management. Reproducibility of thermal wound creation poses a significant challenge. Davidson cites the need to fabricate a custom instrument derived from a common soldering iron, utilizing stackable weights to ensure constant temperature and pressure over a defined time [31]. Accurate modeling and control of

subsequent treatments, debridement and wound wrapping procedures must be controlled with high scrutiny.

Chemical burn creation, in addition to wound reproducibility issues, poses a significant risk of containment. Moreover, substances causing chemical burns in humans do not always affect animal models. One well-characterized model of chemical burn application is the sulphur mustard gas burn. Sulphur mustard causes skin blisters and the development of an ischemic burn wound in both human and porcine skin. In a recent study on debridement techniques, Evison et al described a complex mechanism by which sulphur mustard gas was released within a contained glass cylinder pressed to the intended wound site at a known concentration for a specified time, and then evacuated by an isolated pump system. [29]

Impaired wound healing model to mimic complex human pathology pose an even greater difficulty than other chronic wounds. Animal models for diabetes can be chemically induced or of genetic origin. In murine models, the chemical most commonly used to induce diabetes is streptozotocin (STZ). A dangerous but effective chemical, STZ induces rapid development of diabetes mellitus by selective destruction of the beta-cells in the pancreatic islets. Mice must be fasted at least 12 h prior to injection, and the efficacy of the treatment is highly strain- and dose-dependent. The life span of mice after successful induction of diabetes is limited (several weeks). STZ itself can lead to deleterious effects on macrophage function (known to be part of the wound healing mechanism) [31]. STZ diabetic mouse models have been shown to demonstrate decreased excisional wound closure, reduced granulation tissue formation, and reduced angiogenesis in previous studies. However, the STZ protocol is not suitable for studying the long term effects of diabetes.

Genetic murine models of diabetes pose other difficulties. Arguably, the best characterized murine model of type II diabetes is the db/db (C57B/6J background, known to greatly influence disease progression). The Jackson Labs (Stock No. 000697) description of the

model indicates that a mutation in the leptin receptor gene ($Lepr^{db}$) leads to polyphagia, increased plasma insulin and resulting obesity. Hyperglycemia develops in this model due to hypoinsulinemia and loss of beta cell mass [32]. Widely used as a model of diabetic wound healing, the db/db was shown to exhibit deficiencies in cell-mediated immunity as early as 1978 [33]. Recently, it has been popular in research regarding the topical application of growth factors to model incisional and excisional diabetic wounds [34-36]. While models of type II diabetes are commonly used due to high physiological relevance, reasonably long life span, and subsequent applicability to long-term hyperglycemia-related complications, these mice have a high tendency to be morbidly obese. The dermal fat deposits in loose rodent skin affect the normal mechanisms of closure, creating their own impediment to healing, which affects the accuracy of impaired healing endpoints and requiring the exclusion of mice that become morbidly obese [31].

A non-obese genetic murine model for diabetes mellitus, dubbed the *Akita* mouse may be more useful to study biochemical and histological aspects of diabetic wound healing. The *Akita* mouse shows advantage of early onset of impaired insulin secretion, decreased active beta cell numbers, and a 50% survival time of 305 days [37]. Due primarily to its non-obese characteristics, the *Akita* mouse has been commercially developed and is now publicly available through The Jackson Labs (Stock No. 002207). This model is intended for study of insulin-dependent diabetes mellitus with severe hyperglycemia, further indicating that the model is also accurate for study of diabetic effects on growth factors [38]. Several in depth studies of secondary effects of diabetes by Breyer et al. have used the *Akita* mouse to model diabetic nephropathies with notable success [39]. In a study by Gyurko et al. , chronic hyperglycemia in *Akita* mice showed decreased leukocyte function and increased inflammation. This study speculates that the superoxide production of mitochondria in chronic hyperglycemia contributes to the endothelial damage essential to the long term complications of diabetes. The presence of defects related to

diabetic wound healing impairment strongly supports the use of the *Akita* mouse model in diabetic chronic wound healing [9].

Despite the many advantages of the murine model in reagent availability and both pharmacological and genetic manipulation, the murine model lacks key physiological similarities to human skin. As a more relevant alternative, porcine skin has dermal architecture, vascularity and hair follicle densities, and (nonfunctional) sweat glands similar to human skin [30]. Excisional wounding in the pig produces a limited degree of contraction, in contrast with the dominant effect of this process in murine excisional wounds [31]. In terms of an impaired or chronic wound healing model, however, the pig presents a greater challenge. While specific chemically diabetic pig models (via STZ or alloxan; similar to murine models above) exist and are commercially available (Sinclair Research, Maine), the presence and extent of wound healing impairment, if any, in available diabetic pig models has not yet been characterized [40]. Most of the research cited for these models analyzes vascular changes due to diabetes [41-43]. Glucocorticoid administration offers a viable alternative to induced diabetes in the porcine model that has been used effectively used in studies of impaired cutaneous wound healing in the pig [44, 45]. Glucocorticoids, while known for their anti-inflammatory activity, are also associated with skin thinning and decreased healing capacity, likely due to interference in monocyte differentiation into signaling macrophages or fibroblast collagen synthesis [31].

Ultimately, when studying impaired or chronic wound healing, choice of an animal model is crucial. Precise research scope limitations must be defined before an appropriate model can be selected. Unfortunately, many of the models well-characterized in the literature were developed for the study of pathologies unrelated to cutaneous wound healing. Furthermore, knowledge of the precise mechanisms of wound healing and suspected pathologic basis of impairment is crucial to selecting a model that can yield applicable results.

Enhanced Wound Healing

Recent work in wound healing has seen a certain degree of paradigm shift from the attempted shutdown of natural bodily mechanisms to a situation in which therapies are attempting to increase or stimulate the activity of known pathways. The majority of treatments currently in development to enhance wound healing, especially targeted towards the impaired or chronic wound, are based on the use of topical gels containing potent mixtures natural wound healing-associated growth factors. In a review about the use of growth factors in ulcer treatment, Bennett concludes that limited numbers for human trials as well as inconsistent endpoints between trials preclude drawing any firm conclusions. These mixed results are not surprising given the precise regulation in time and space of growth factors and cytokines associated with normal wound healing. Bennett also cites that the best treatment method available is still traditional care and mechanical debridement, but that expensive gel-based treatments may eventually offer a significant alternative despite cost due to revascularization results [18]. Other significant efforts have also led to the creation of extended release gels and compounds that target the chemical acceleration of debridement, in an attempt to decrease the loss of healthy tissue lost to traditional mechanisms [30].

Lasers for Wound Healing Enhancement

While most efforts focus on the use of results from the mechanistic studies of wound healing to create chemical compounds to aid healing or prevent deleterious byproducts of chronic wounds, some work focuses on the upregulation of natural pathways without the addition of potent chemical substances. In these methods, lasers are used as a source of non-contact dermal heating through the selective absorption of light. While indubitably less expensive in long term care than the exogenous development and topical application of growth factors, the thermal

regulation of wound healing mechanisms is also arguably more customizable to meet specific patient needs.

A series of studies by Beckham et al. and Wilmink et al. indicate that optimized doses of laser light are sufficient to upregulate the induction of stress protein HSP70 (heat shock protein 70). The studies utilized bioluminescent imaging to optimize the dose of light that maximized the heat shock protein induction. The treatment has been shown to protect against subsequent thermal injury, and accelerate the healing of subsequent cutaneous wounds. Analysis indicated increased maximum wound tensile load, cellular proliferation, increased local circulation.[46, 47]

Confirming the induction of HSP 70 in laser dermal treatments, work by Capon et al. and Souil et al. focused more on a treatment designed to accelerate wound closure with endpoints aimed toward the structural and cosmetic benefits of minimal scarring after surgery [48-50]. While the former is likely more applicable to the treatment of impaired wound healing scenarios, the latter confirms the applicability of the treatment after the creation of the wound. Despite confirmation of the presence of HSP70, and correlation between its upregulation and enhanced dermal wound healing, the mechanism behind the action of the treatment is unknown.

Unlike other methods for inducing tissue heating, lasers allow fast heat deposition, uniform heat distribution, and therefore highly controlled spatial-temporal tissue heating. In addition, laser energy can be delivered through optical fibers, allowing for high precision heating and relative ease of use. While one could reasonably argue that the same thermal induction and subsequent HSP 70 induction could be achieved by inexpensive contact methods, the physical contact required for conduction is not optimal for the treatment existing ulcerated or burn wounds. In contrast, laser light can be delivered in non-contact fashion, thus mitigating risks of infection and pain due to contact with an open wound.

Lasers provide more than simply a non-contact heating method. In the context of thermal enhancement of dermal wound healing, lasers function through a principle of selective

absorption. Tissue chromophores, molecules that absorb light, each have an intrinsic absorption spectrum, such that the probability of light absorption by a given chromophore depends directly on the wavelength, in a manner that can accurately be modeled by simulation [51]. This absorbed energy is converted to heat, which diffuses according to tissue physical and thermal properties [52]. For successful thermal enhancement, the laser parameters must be matched to both tissue optical and physical properties [53]. With proper understanding of the properties and mechanisms of laser-tissue interactions, laser treatments can be tailored to generate a desired "dose" of light and control subsequent heat generation as a function of time and space. These treatments can then be optimized to ensure desired heating while minimizing tissue damage.

Heat Shock Proteins in Wound Healing

Cellular responses to thermal stress involve complex pathways that are noted for their transcriptional activation of heat shock protein (HSP) genes. Transcriptional activation can be seen immediately after thermal insult and follows a characterized time course. A large family of diversified proteins, HSP's are ubiquitous and conserved in most species [54-57]. HSP's have been shown to maintain cellular homeostasis through mechanisms involving new protein folding and refolding of denatured protein.

The very process of transcription places nascent proteins at risk. During synthesis, newly formed segments of protein have not yet folded to achieve entropically favorable charge balance. HSP's shield highly hydrophobic linear regions of transcribed polypeptides, preventing interaction with cytosolic proteins and the subsequent aggregation that prevents functional folding [58]. Through similar methods, HSP's assist in the refolding of denatured proteins. Though explained to a lesser extent, loss of cytosolic protein function through chemical or thermal denaturation leads to the upregulation of HSP's. The cylindrical domains of the HSP envelope the denatured protein, providing an environment favorable to proper refolding [58].

Through molecular mechanisms involving mitochondrial signaling and caspase-3, HSP's are also responsible for protective processes, shielding cells from subsequent injury and apoptosis (see **Figure 3**) [59]. For these reasons, HSP's are widely considered a primary family of "chaperone" proteins.

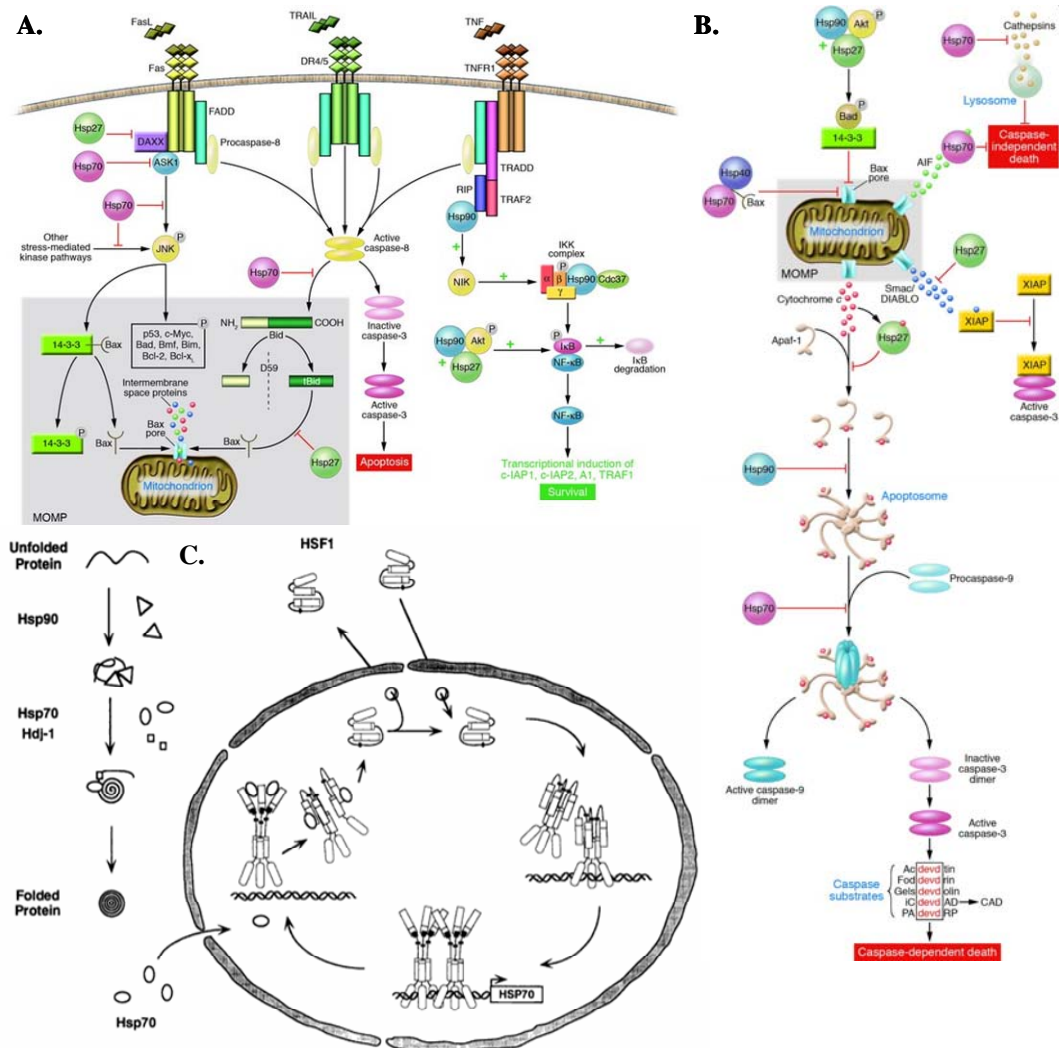


Figure 3. The molecular pathways and regulations of prominent HSPs. A indicates the activity of multiple HSPs in the prevention of three prominent apoptotic cascades between the cell-surface receptor binding level and the mitochondrial signaling level [59]. B highlights the involvement of HSPs subsequent to mitochondrial signaling, affecting both caspase dependent and caspase independent apoptotic pathways [59]. C illustrates the upregulation mechanism of HSP70 through HSF1 in response to protein denaturation [63, 64].

Of particular interest, HSP70 exists in most cells under normal condition, but is noted for its highly inducible expression kinetics, cited as high as 15% of cellular protein content [60]. Unlike other HSP's, HSP70 lacks a cylindrical domain, and is instead considered a holding protein that participates in refolding through the temporary binding of short amino acid regions[58]. HSP70 is known to refold unfolded proteins through ATP cycling mechanisms [58, 61]. The complicated mechanism of HSP70 upregulation suggests how the protein helps protect from repetitive insult. Under normal conditions HSP70 is complexed with its own heat shock transcription factor, HSF1. Under stress, HSP70 releases from complex to participate in refolding, while allowing HSF1 to participate in transcription (see **Figure 3.C**) [62]. Upon completion of refolding, HSP70 again complexes with HSF1, providing feedback inhibition and an increase in the stable population of HSP70 [63, 64]. The protective mechanisms of HSP70 are closely associated with the cell life cycle and the control of apoptosis (see **Figure 3**). The induction of HSP70 has been shown to inhibit cell death and promote cell survival in response to insult [65-68].

Beyond response to thermal insult, HSP upregulation by inflammatory cells has been shown during early wound healing, speculated to be a protection mechanism against oxidative stress [69]. In impaired wound healing conditions, HSP70 induction is substantially diminished [70]. The coordination between HSP's and inflammation has been thoroughly studied, but no definitive mechanism of action has been determined. HSP activity is known to correlate to decreased activity of well-characterized pro-inflammatory mediators including IL-1 β and TNF α . [71]. Various key biological chemicals have been shown to modulate HSP activity, including prostaglandins and many non-steroidal anti-inflammatory agents [72, 73]. Though HSP's and HSP70 in particular have been shown to have protective effects related to wound healing, their regulation is clouded by complex overlapping pathways at the heart of cell survival. Though it will be difficult to experimentally determine a mechanism of action for a protein so

integral to cell survival (many interacting proteins listed will not yield viable knockouts), understanding how this protein family enhances wound healing will be crucial to the use of HSP modulation to improve impaired wound healing through intrinsic mechanisms.

Optical Analysis of Wound Healing: Raman Spectroscopy

In the efforts to determine mechanisms of impaired and enhanced dermal wound healing to increase treatment efficacy, the current standard measurements in pathology studies (tensiometry, histology, and biochemical assays) would require a significant amount of animal sacrifice, while resulting data would be based on the underlying assumptions that the response shown throughout several time points is the same between organisms. Moreover, these methods of data collection, though well established in the literature, do not translate to clinical studies. The use of an optical spectroscopy may be able to effectively eliminate those variables while gathering an in vivo spatial-temporal localization of biochemical content, through techniques that are currently used clinically.

Raman scattering is an inelastic scattering phenomenon that occurs when a photon scatters off an anisotropic chemical bond, resulting in a vibrational level energy change and a subsequent shift in wavenumber (see **Figure 4.e,f**) [74]. Because the energy change is dependent upon the chemical bond encountered and not a function of initial photon wavelength, Raman Spectroscopy (RS) offers a distinct advantage over other optical spectroscopic modalities, in that it yields the same information regardless of input wavelength. However, Raman scattering is probabilistically unlikely relative to other light-tissue interactions and suffers under the burden of needing high collection efficiency and interference from other interactions including fluorescence. Careful choice of wavelength sources and established preprocessing algorithms allows for the elimination of interference and the construction of a spectrum of Raman

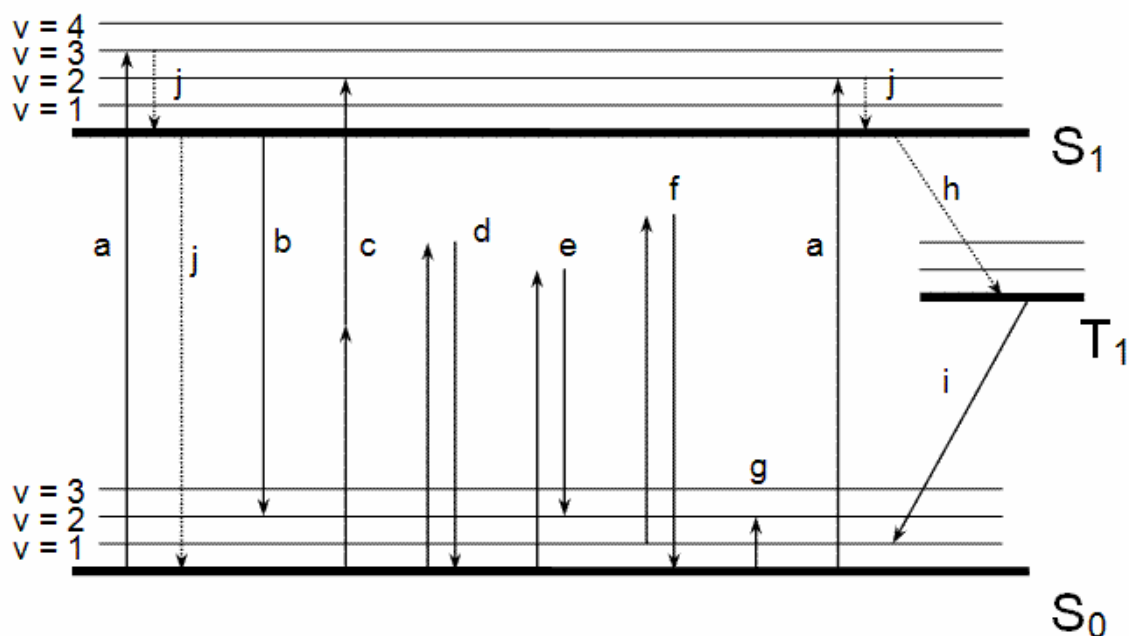


Figure 4. Jablonski Diagram of Vibrational Spectroscopies: a one-photon electronic absorption; b fluorescence; c two-photon electronic absorption; d Rayleigh scattering; e Stokes Raman scattering; f anti-Stokes Raman scattering; g one-photon vibrational absorption; h intersystem crossing (NRT); i phosphorescence; j internal conversion (NRT)

*NRT: Non Radiative Transition

Adapted from Iari-Gabriel Marino's "Vibrational Spectroscopy" at http://www.fis.unipr.it/~marino/08_spectroscopy.html

wavenumber shifts. Such a spectrum naturally represents the biochemical distribution of bonds encountered in the sample.

The use of Raman Spectroscopy as an optical tool has been developed for decades in the field of analytical chemistry, especially for the examination of pharmaceutical quality [75]. During this time, interest in using Raman to analyze biological compounds grew, but efforts were largely limited by technological capability. The analysis of purified compounds, molecules, and cultured cells indicated that Raman was sensitive to conformational changes and capable of distinguishing features of biochemical content. Raman spectra of nucleic acids were sensitive to DNA conformational forms (A,B,C, and Z), backbone organization, and the relative contributions of specific base pairs, even distinguishing differences in phosphate stretching between DNA and RNA [74]. Developments of near infrared (NIR) laser sources designed for Raman spectroscopy

minimize the impact of tissue fluorescence on collection, allowing for feasible application to a wide variety of biomedical problems; however, relatively few have pursued the use of Raman Spectroscopy to tissue applications or in vivo studies [76-78].

Several specialized tissues make ideal environments for the use of RS as a quantitative measure of disease. Römer et al. have pursued the use of NIR Raman for the study of arteries and atherosclerosis [79]. The artery itself is composed of distinct, relatively homogeneous layers in the absence of atherosclerotic disease. Crucially, the progression of atherosclerotic disease is not based upon the size or shape of lesions, but more importantly a function of content. Ultimately, their classification algorithm was able to correctly classify 64 out of 68 samples as a function of cholesterol content and calcified salts. Analysis also indicated the ability to deconvolve the Raman spectra to estimate the relative contribution of diseased and normal components, confirming Raman Spectroscopy sensitivity and providing quantitative measures of plaque content [79].

The investigation of bone and related hard tissue provides an idyllic match to the strengths of RS. Bone is composed primarily of hydroxyapatite crystals and collagen, making it relatively pure in comparison to many soft tissues; however, slight variations of composition and formation lead to significant changes in functional strength and risk for failure. The narrow spectral features of RS, coupled with the detection of both inorganic and organic components, allows for detailed analysis of mineral-matrix interactions. Studies of the Raman spectra of bone have been conducted for disease states, growth and repair, as well as for the evaluation of synthetic biomaterials [80]. More recently, RS has even been used to investigate the effect of differential genetic expression on bone development through mouse model knockout of matrix metalloproteinases [81].

While the strengths of Raman Spectroscopy match analysis needs of certain pure or specialized tissues, the analysis of heterogeneous soft tissues provides a greater challenge. The

increase in heterogeneity broadens many spectral features, while potentially increasing the number of fluorophores obscuring the signal. Nevertheless, the use of NIR Raman spectroscopy has led to significant success in the diagnosis of complex diseases including breast and cervical cancer [72, 74, 77, 82-84]. A novel statistical method for multiclass analysis of Raman spectra developed in our lab combines the method of maximum representation and discrimination feature (MRDF) to extract diagnostic information with sparse multinomial logistic regression (SMLR) to classify spectra based on nonlinear features [85]. In a recent study of cervical dysplasia, this method correctly classified 95% of high-grade spectra and 74% of low-grade data, with both sensitivity and specificity above 95% [85].

Owing perhaps to accessibility, the study of skin using Raman Spectroscopy is also largely motivated by the numerous debilitating skin diseases that could be properly treated or even cured if diagnosed or assessed early in development. Skin lesions are usually isolated and often non-invasive, but rare invasive cases are highly infiltrative and can require surgical intervention. The development of confocal and fiber optic Raman instrumentation represents the potential for real-time surgical guidance, and subsequent decreases in procedure cost and patient recovery time [76, 86]. Raman Spectroscopy has also been used to correlate the putative antioxidant role of skin carotenoids to cancerous lesion prevention [87]. In cosmetic applications, confocal Raman microspectroscopy has been used *in vivo* to demonstrate a depth-dependent distribution of natural moisturizing factor, a well-characterized byproduct of enzymatic degradation to preserve moisture in the stratum corneum in dry environments [86]. The diversity of successful applications of Raman Spectroscopy to skin supports the hypothesis that Raman Spectroscopy could viably be used for *in vivo* analysis of cutaneous wound healing.

Despite the possibility of a natural extension of ongoing studies in bone or skin, remarkably few research groups have pursued the investigation of wound healing or tissue repair using optical spectroscopies. Zhang et al. utilized the relative strengths of both Infrared (IR)

Spectroscopy and confocal Raman spectroscopy to visualize the keratin-rich reepithelialization front and the spatial distribution of elastin and collagen within the wound bed, respectively [88]. Chan et al. analyzed an ex vivo human skin wound culture model with IR and confocal Raman spectroscopies over several days. Subsequent deconvolution of confocal mappings using factors with distinct elastin and collagen features allowed for spatial-temporal distribution of major structural proteins [89]. Crane et al. presented at the 2008 conference of the Federation of Analytical Chemistry and Spectroscopy Societies (FACSS) about Raman studies of wound biopsies from soldiers, demonstrating qualitative differences between healing and chronic wound spectra [90]. Alimova et al. analyzed the changes in spectral content as a function of incisional wound closure via traditional suture or experimental laser tissue welding from two different lasers at discrete time points in the healing process of four guinea pigs [91]. This work differs from other reports of spectroscopic wound healing in several ways. The Raman spectroscopy acquisition protocol for this study utilizes irradiances and collection times currently approved for clinical study. This work represents the first known report of Raman sensitivity to spectral differences in the healing wound and neighboring tissue as a function of both genetic expression as well as treatment response.

The collection of a clinically relevant, in vivo profile of healing wounds was possible due to unique system design. The use of Raman Spectroscopy coupled to microscope systems has been used at length to examine histological sections in vitro with existing commercial systems [75]. However, our lab utilizes a fiber optic probe design in combination with a fast acquisition protocol and automated pre-processing to make a portable, clinically feasible Raman system. The portable Raman system consists of a mode locked diode laser ($\lambda=785\text{nm}$; Innovative Photonic Solutions, Mammoth Junction, NJ) coupled to a custom fiber optic probe (7 collection fibers surrounding an excitation fiber; Emvision, Loxahatchee, FL). 80 mW power output from the excitation fiber provides sufficient signal at irradiances that do not induce significant heating of

the tissue. Collection fibers are coupled to a $f/1.8$ holographic imaging spectrograph (Kaiser Optical Systems, Inc., Ann Arbor, MI), subsequently focusing light onto a back-illuminated, deep depletion, thermo-electrically cooled Andor Newton CCD (Andor Technologies plc., Belfast, UK). For most skin applications, each Raman scan consists of 3 accumulations of 3 second exposures of the CCD to ensure maximum signal without saturation.

Many biological substances can be detected as an intensity "fingerprint" of Raman shift peaks [75]. Complexity increases in living tissue, given the presence of numerous fluorophores. Once the isolated Raman shift spectra have been obtained, the relative concentrations of individual "Raman active" species can be detected. Occasionally, specific diagnostic peaks can be isolated to indicate the presence of pathological effect or the relative concentration (intensity) of an important protein. In thoroughly characterized situations, a library of peak signatures indicative of known prevalent molecules is used in combination with advanced regression analysis to deconvolve the composite Raman signal into relative concentrations [92, 93].

In the use of Raman spectroscopy for wound healing analysis, such that no specific substance indicative of normal or impaired wound healing is yet known, the latter technique may be required. The review of ECM proteins represents the major volume constituents of the acellular components of skin. These will likely be responsible for a large portion of the signal observed in vivo. Given that many of these proteins have similar repeating structural domains, and differ primarily in posttranslational modifications and functionalized ends, the isolated Raman spectra of these substances would be invaluable in determining differences in the progression between normal, impaired, and enhanced wound repair. A broad bank of literature supports the assignment of Raman wavenumbers to chemical bonds related to inflammation and extracellular matrix proteins due to their relevance to cancer studies [74, 84, 94, 95], subsequently allowing for ease of analysis in related wound healing parameters.

One of the primary obstacles to measuring Raman spectra of the healing wound will be obtaining information below the highly absorptive scab region. Spatially Offset Raman Spectroscopy (SORS) operates on the probabilistic principles of light scattering that correlate translational path length to the average depth reached by the scattered photon. Over a large number of photons, the further the photons are collected from the source of incidence, the deeper the level of biochemical information resolved [75]. SORS may help to collect the necessary information to determine the biochemical content of a healing wound.

Summary

In this thesis, I demonstrate the use of Raman Spectroscopy as a quantitative analytical method to assess the role of HSP70 in incisional wound healing, as well as the relationship between HSP70 and a previously established laser preconditioning protocol. The overall goal of this thesis is to determine whether HSP70, previously used only as a biomarker for optimization, plays an active role in the mechanism of laser preconditioning therapy. The specific aims include: establishment of a Raman spectral profile of murine incisional wound healing; assess differences in the wound healing profile as a function of hsp70; quantification and qualification of downstream effects of laser preconditioning through spectral profile analysis. The next chapter of this work delineates the specific methods and results of the experimental study. The final chapter will provide a detailed discussion of the scope of both the results and conclusions of the study, as well as future directions for this work. The success of this work not only suggests the degree of involvement for HSP70 in wound healing and laser preconditioning, but it also implies the potential of Raman Spectroscopy as quantitative method for the diagnosis of wounds and noninvasive assessment of treatment response.

Works Cited:

1. Davidson, J.M. and S.I. Benn, *Biochemical and molecular regulation of angiogenesis and wound repair*. In: Cellular and Molecular Pathogenesis, A.E. Sirica (ed), Raven Press, New York, 1996: p. 79-108.
2. Braddock, M., C.J. Campbell, and D. Zuder, *Current therapies for wound healing: electrical stimulation, biological therapeutics, and the potential for gene therapy*. Int J Dermatol, 1999. **38**(11): p. 808-17.
3. Martin, P., *Wound healing--aiming for perfect skin regeneration*. Science, 1997. **276**(5309): p. 75-81.
4. Matousek, S., A.K. Deva, and R. Mani, *Outcome measurements in wound healing are not inclusive: a way forward*. Int J Low Extrem Wounds, 2007. **6**(4): p. 284-90.
5. Harris, M.I., et al., *Prevalence of diabetes, impaired fasting glucose, and impaired glucose tolerance in U.S. adults. The Third National Health and Nutrition Examination Survey, 1988-1994*. Diabetes Care, 1998. **21**(4): p. 518-24.
6. Frykberg, R.G., *Epidemiology of the diabetic foot: ulcerations and amputations*. Adv Wound Care, 1999. **12**(3): p. 139-41.
7. Ashcroft, G.S. and S.J. Mills, *Androgen receptor-mediated inhibition of cutaneous wound healing*. J Clin Invest, 2002. **110**(5): p. 615-24.
8. Eming, S.A., T. Krieg, and J.M. Davidson, *Inflammation in wound repair: molecular and cellular mechanisms*. J Invest Dermatol, 2007. **127**(3): p. 514-25.
9. Gyurko, R., et al., *Chronic hyperglycemia predisposes to exaggerated inflammatory response and leukocyte dysfunction in Akita mice*. J Immunol, 2006. **177**(10): p. 7250-6.
10. Kumar, V., et al., *Robbins and Cotran pathologic basis of disease*. 2005, Philadelphia: Elsevier Saunders.
11. Davidson, J., *Class Notes: Pathology 335: Diseases of the Extracellular Matrix*. 2008.
12. McKusick, V., *Heritable Disorders in Connective Tissue*. 1956, St. Louis: Mosby.
13. Loots, M.A.M., et al., *Differences in Cellular Infiltrate and Extracellular Matrix of Chronic Diabetic and Venous Ulcers Versus Acute Wounds*. Journal of Investigative Dermatology, 1998. **111**(5): p. 850-857.
14. Valenick, L.V., H.C. Hsia, and J.E. Schwarzbauer, *Fibronectin fragmentation promotes alpha4beta1 integrin-mediated contraction of a fibrin-fibronectin provisional matrix*. Exp Cell Res, 2005. **309**(1): p. 48-55.
15. Alberts, B.J., A; Lewis, J; Raff, M; Roberts, P; Walter, P, *Molecular Biology of the Cell*. 4 ed. 2002: Garland Science.
16. Schaffer, M., et al., *Nitric oxide restores impaired healing in normoglycaemic diabetic rats*. J Wound Care, 2007. **16**(7): p. 311-6.
17. Bennet, S.P. and e. al., *Growth factors in the treatment of diabetic foot ulcers*. British Journal of Surgery Society Ltd, 2003. **2003**(90): p. 133-146.
18. S.P. Bennet, e.a., *Growth factors in the treatment of diabetic foot ulcers*. British Journal of Surgery Society Ltd, 2003. **2003**(90): p. 133-146.
19. Lipsky, B.A., et al., *Diagnosis and treatment of diabetic foot infections*. Clin Infect Dis, 2004. **39**(7): p. 885-910.
20. Lipsky, B.A., et al., *Diagnosis and treatment of diabetic foot infections*. Plast Reconstr Surg, 2006. **117**(7 Suppl): p. 212S-238S.

21. Eldor, R., et al., *New and experimental approaches to treatment of diabetic foot ulcers: a comprehensive review of emerging treatment strategies*. Diabet Med, 2004. **21**(11): p. 1161-73.
22. Ablaza, V. and J. Fisher, *Telemedicine and wound care management*. Home Care Provid, 1998. **3**(4): p. 206-11; quiz 212-3.
23. Wu, S.C., et al., *Foot ulcers in the diabetic patient, prevention and treatment*. Vasc Health Risk Manag, 2007. **3**(1): p. 65-76.
24. Eming, S.A., et al., *Particle-mediated gene transfer of PDGF isoforms promotes wound repair*. J Invest Dermatol, 1999. **112**(3): p. 297-302.
25. Benn, S.I., et al., *Particle-mediated gene transfer with transforming growth factor-beta1 cDNAs enhances wound repair in rat skin*. J Clin Invest, 1996. **98**(12): p. 2894-902.
26. Brem, H., et al., *Evidence-based protocol for diabetic foot ulcers*. Plast Reconstr Surg, 2006. **117**(7 Suppl): p. 193S-209S; discussion 210S-211S.
27. Kauvar, D.S., et al., *Burns sustained in combat explosions in Operations Iraqi and Enduring Freedom (OIF/OEF explosion burns)*. Burns, 2006. **32**(7): p. 853-7.
28. Owens, B.D., et al., *Combat wounds in operation Iraqi Freedom and operation Enduring Freedom*. J Trauma, 2008. **64**(2): p. 295-9.
29. Evison, D., R.F. Brown, and P. Rice, *The treatment of sulphur mustard burns with laser debridement*. J Plast Reconstr Aesthet Surg, 2006. **59**(10): p. 1087-93.
30. Bott, R., et al., *A silicone-based controlled-release device for accelerated proteolytic debridement of wounds*. Wound Repair Regen, 2007. **15**(2): p. 227-35.
31. Davidson, J.M., *Animal models for wound repair*. Arch Dermatol Res, 1998. **290** Suppl: p. S1-11.
32. *JAX Mice Database - 000697 B6.Cg-m +/+ Lepr<db>/J*. 2008 [cited; Available from: <http://jaxmice.jax.org/strain/000697.html>].
33. Mandel, M.A. and A.A. Mahmoud, *Impairment of cell-mediated immunity in mutation diabetic mice (db/db)*. J Immunol, 1978. **120**(4): p. 1375-7.
34. Cho, C.H., et al., *COMP-angiopoietin-1 promotes wound healing through enhanced angiogenesis, lymphangiogenesis, and blood flow in a diabetic mouse model*. Proc Natl Acad Sci U S A, 2006. **103**(13): p. 4946-51.
35. Mellin, T.N., et al., *Acidic fibroblast growth factor accelerates dermal wound healing in diabetic mice*. J Invest Dermatol, 1995. **104**(5): p. 850-5.
36. Obara, K., et al., *Acceleration of wound healing in healing-impaired db/db mice with a photocrosslinkable chitosan hydrogel containing fibroblast growth factor-2*. Wound Repair Regen, 2005. **13**(4): p. 390-7.
37. Yoshioka, M., et al., *A novel locus, Mody4, distal to D7Mit189 on chromosome 7 determines early-onset NIDDM in nonobese C57BL/6 (Akita) mutant mice*. Diabetes, 1997. **46**(5): p. 887-94.
38. Puolakkainen, P.A., et al., *Acceleration of wound healing in aged rats by topical application of transforming growth factor-beta(1)*. Wound Repair Regen, 1995. **3**(3): p. 330-9.
39. Breyer, M.D., *Animal Models of Diabetic Complications Consortium: Update Report, in Online <http://www.amdcc.org/documents/reports/BreyerAR2004.pdf>*.
40. Reed, M.J., et al., *Age-related differences in repair of dermal wounds and myocardial infarcts attenuate during the later stages of healing*. In Vivo, 2006. **20**(6B): p. 801-6.
41. Boodhwani, M., et al., *Functional, cellular, and molecular characterization of the angiogenic response to chronic myocardial ischemia in diabetes*. Circulation, 2007. **116**(11 Suppl): p. I31-7.

42. Dixon, J.L., et al., *Dyslipidemia and vascular dysfunction in diabetic pigs fed an atherogenic diet*. *Arterioscler Thromb Vasc Biol*, 1999. **19**(12): p. 2981-92.
43. Roberts, T.M., et al., *Alterations in the oxidative metabolic profile in vascular smooth muscle from hyperlipidemic and diabetic swine*. *Mol Cell Biochem*, 2001. **217**(1-2): p. 99-106.
44. Quaglino, D., Jr., et al., *Transforming growth factor-beta stimulates wound healing and modulates extracellular matrix gene expression in pig skin: incisional wound model*. *J Invest Dermatol*, 1991. **97**(1): p. 34-42.
45. Quaglino, D., Jr., et al., *Transforming growth factor-beta stimulates wound healing and modulates extracellular matrix gene expression in pig skin. I. Excisional wound model*. *Lab Invest*, 1990. **63**(3): p. 307-19.
46. Beckham, J.T., et al., *Assessment of cellular response to thermal laser injury through bioluminescence imaging of heat shock protein 70*. *Photochem Photobiol*, 2004. **79**(1): p. 76-85.
47. Wilmink, G.J., et al., *Assessing laser-tissue damage with bioluminescent imaging*. *J Biomed Opt*, 2006. **11**(4): p. 041114.
48. Souil, E., et al., *Treatment with 815-nm diode laser induces long-lasting expression of 72-kDa heat shock protein in normal rat skin*. *Br J Dermatol*, 2001. **144**(2): p. 260-6.
49. Capon, A., et al., *Laser assisted skin closure (LASC) by using a 815-nm diode-laser system accelerates and improves wound healing*. *Lasers Surg Med*, 2001. **28**(2): p. 168-75.
50. Capon, A.C., et al., *Scar prevention by laser-assisted scar healing (LASH): a pilot study using an 810-nm diode-laser system*. *Lasers Surg Med*, 2008. **40**(7): p. 443-5.
51. Wang, L., and Wu H, *Biomedical Optics: Principles and Imaging* 1ed. 2007: Wiley-Interscience.
52. Vogel, A. and V. Venugopalan, *Mechanisms of pulsed laser ablation of biological tissues*. *Chem Rev*, 2003. **103**(2): p. 577-644.
53. Welch, A.J., and van Gemert, MJC, *Optical-Thermal Response of Laser-Irradiated Tissue*. 1995, New York: Plenum.
54. Diller, K.R., *Stress protein expression kinetics*. *Annu Rev Biomed Eng*, 2006. **8**: p. 403-24.
55. Mayer, M.P. and B. Bukau, *Hsp70 chaperones: cellular functions and molecular mechanism*. *Cell Mol Life Sci*, 2005. **62**(6): p. 670-84.
56. Young, J.C., et al., *Pathways of chaperone-mediated protein folding in the cytosol*. *Nat Rev Mol Cell Biol*, 2004. **5**(10): p. 781-91.
57. Young, J.C., J.M. Barral, and F. Ulrich Hartl, *More than folding: localized functions of cytosolic chaperones*. *Trends Biochem Sci*, 2003. **28**(10): p. 541-7.
58. Frydman, J., *Folding of newly translated proteins in vivo: the role of molecular chaperones*. *Annu Rev Biochem*, 2001. **70**: p. 603-47.
59. Beere, H.M., *Death versus survival: functional interaction between the apoptotic and stress-inducible heat shock protein pathways*. *The Journal of Clinical Investigation*, 2005. **115**(10): p. 2633-2639.
60. Pockley, A.G., *Heat shock proteins, inflammation, and cardiovascular disease*. *Circulation*, 2002. **105**(8): p. 1012-7.
61. Nollen, E.A., et al., *In vivo chaperone activity of heat shock protein 70 and thermotolerance*. *Mol Cell Biol*, 1999. **19**(3): p. 2069-79.
62. Morris, S.D., *Heat shock proteins and the skin*. *Clin Exp Dermatol*, 2002. **27**(3): p. 220-4.

63. Kiang, J.G. and G.C. Tsokos, *Heat shock protein 70 kDa: molecular biology, biochemistry, and physiology*. Pharmacol Ther, 1998. **80**(2): p. 183-201.
64. Morimoto, R.I., P.E. Kroeger, and J.J. Cotto, *The transcriptional regulation of heat shock genes: a plethora of heat shock factors and regulatory conditions*. Exs, 1996. **77**: p. 139-63.
65. Samali, A. and T.G. Cotter, *Heat shock proteins increase resistance to apoptosis*. Exp Cell Res, 1996. **223**(1): p. 163-70.
66. Bowman, P.D., et al., *Survival of human epidermal keratinocytes after short-duration high temperature: synthesis of HSP70 and IL-8*. Am J Physiol, 1997. **272**(6 Pt 1): p. C1988-94.
67. Mosser, D.D., et al., *Role of the human heat shock protein hsp70 in protection against stress-induced apoptosis*. Mol Cell Biol, 1997. **17**(9): p. 5317-27.
68. Jaattela, M., et al., *Major heat shock protein hsp70 protects tumor cells from tumor necrosis factor cytotoxicity*. Embo J, 1992. **11**(10): p. 3507-12.
69. McMurtry, A.L., et al., *Expression of HSP70 in healing wounds of diabetic and nondiabetic mice*. J Surg Res, 1999. **86**(1): p. 36-41.
70. Wong, H.R., *Potential protective role of the heat shock response in sepsis*. New Horizons-the Science and Practice of Acute Medicine, 1998. **6**(2): p. 194-200.
71. Leppa, S. and L. Sistonen, *Heat shock response - Pathophysiological implications*. Annals of Medicine, 1997. **29**(1): p. 73-78.
72. Majumder, S.K., et al., *Comparison of autofluorescence, diffuse reflectance, and Raman spectroscopy for breast tissue discrimination*. J Biomed Opt, 2008. **13**(5): p. 054009.
73. Patil, C.A., et al., *Combined Raman spectroscopy and optical coherence tomography device for tissue characterization*. Opt Lett, 2008. **33**(10): p. 1135-7.
74. Mahadevan-Jansen, A. and R.R. Richards-Kortum, *Raman spectroscopy for the detection of cancers and precancers*. Journal of Biomedical Optics, 1996. **1**(1): p. 31-70.
75. Matousek, P., *Deep non-invasive Raman spectroscopy of living tissue and powders*. Chem Soc Rev, 2007. **36**(8): p. 1292-304.
76. Nijssen, A., et al., *Towards oncological application of Raman spectroscopy*. J Biophotonics, 2009. **2**(1-2): p. 29-36.
77. Kanter, E.M., et al., *Application of Raman spectroscopy for cervical dysplasia diagnosis*. J Biophotonics, 2009. **2**(1-2): p. 81-90.
78. Hanlon, E.B., et al., *Prospects for in vivo Raman spectroscopy*. Phys Med Biol, 2000. **45**(2): p. R1-59.
79. Romer, T.J., et al., *Histopathology of human coronary atherosclerosis by quantifying its chemical composition with Raman spectroscopy*. Circulation, 1998. **97**(9): p. 878-85.
80. Carden, A. and M.D. Morris, *Application of vibrational spectroscopy to the study of mineralized tissues (review)*. Journal of Biomedical Optics, 2000. **5**(3): p. 259-268.
81. Bi, X., et al. *Raman spectroscopy for assessment of bone quality in MMP-2 knockout mice*. in *Optics in Bone Biology and Diagnostics*. 2009. San Jose, CA, USA: SPIE.
82. Kanter, E.M., et al., *Effect of hormonal variation on Raman spectra for cervical disease detection*. Am J Obstet Gynecol, 2009. **200**(5): p. 512 e1-5.
83. Keller, M.D., et al., *Detecting temporal and spatial effects of epithelial cancers with Raman spectroscopy*. Dis Markers, 2008. **25**(6): p. 323-37.
84. Mahadevan-Jansen, A., et al., *Near-infrared Raman spectroscopy for in vitro detection of cervical precancers*. Photochem Photobiol, 1998. **68**(1): p. 123-32.
85. Kanter, E.M., et al., *Multiclass discrimination of cervical precancers using Raman spectroscopy*. Journal of Raman Spectroscopy, 2009. **40**(2): p. 205-211.

86. Caspers, P.J., et al., *In Vivo Confocal Raman Microspectroscopy of the Skin: Noninvasive Determination of Molecular Concentration Profiles*. Journal of Investigative Dermatology, 2001. **116**(3): p. 434-442.
87. Darvin, M.E., et al., *Influence of IR radiation on the carotenoid content in human skin*. Optics and Spectroscopy, 2009. **107**(6): p. 917-920.
88. Zhang, G., et al., *Parallel studies of cutaneous wound healing: IR imaging, confocal Raman microscopy, and molecular biology*. Journal of Investigative Dermatology, 2009. **129**: p. 40.
89. Chan, K.L.A., et al., *A coordinated approach to cutaneous wound healing: vibrational microscopy and molecular biology*. Journal of Cellular and Molecular Medicine, 2008. **12**(5B): p. 2145-2154.
90. Crane, N.J., et al. *Raman Spectroscopic Analysis of Warrior Wound Biopsies: What Happens When Good Wounds Go Bad?* in *The Federation of Analytical Chemistry and Spectroscopy Societies - Bioanalytical-Raman*. 2008.
91. Alimova, A., et al., *In vivo molecular evaluation of guinea pig skin incisions healing after surgical suture and laser tissue welding using Raman spectroscopy*. Journal of Photochemistry and Photobiology B-Biology, 2009. **96**(3): p. 178-183.
92. Buschman, H.P., et al., *Raman microspectroscopy of human coronary atherosclerosis: biochemical assessment of cellular and extracellular morphologic structures in situ*. Cardiovasc Pathol, 2001. **10**(2): p. 69-82.
93. Motz, J.T., et al., *In vivo Raman spectral pathology of human atherosclerosis and vulnerable plaque*. J Biomed Opt, 2006. **11**(2): p. 021003.
94. Lieber, C.A., et al., *Raman microspectroscopy for skin cancer detection in vitro*. J Biomed Opt, 2008. **13**(2): p. 024013.
95. Lieber, C.A., et al., *In vivo nonmelanoma skin cancer diagnosis using Raman microspectroscopy*. Lasers Surg Med, 2008. **40**(7): p. 461-7.

CHAPTER II

IN VIVO ANALYSIS OF LASER PRECONDITIONING IN INCISIONAL WOUND HEALING OF WILD-TYPE AND HSP70 KNOCKOUT MICE WITH RAMAN SPECTROSCOPY

Alex Makowski¹, Jeffrey Davidson², Anita Mahadevan-Jansen¹, E. Duco Jansen¹

¹Department of Biomedical Engineering, Vanderbilt University, ²Department of Pathology, Vanderbilt University

Abstract:

Laser preconditioning augments incisional wound healing by reducing scar tissue and increasing maximum tensile load of the healed wound. While the exact role of HSP70 in this process has not been clearly elucidated, it is well established that HSP70 expression is correlated with thermal stress and subsequent repair as part of the thermal (pre)conditioning response. Recent studies have optimized treatments or confirmed results using HSP70 as a biomarker. Under the hypothesis that HSP70 plays an active role in reported results and to better understand the downstream effects of laser preconditioning, this study utilized a probe-based Raman spectroscopy system to achieve an in-vivo, spatio-temporal biochemical profile of murine skin incisional wounds as a function of laser preconditioning and the presence of HSP70. Raman spectra yielded significant differences (t-test; $\alpha=.05$) in several known biochemical peaks between wild-type (WT) and HSP70 knockout mice on wounds and in adjacent tissue early in the wound healing process. Analysis of peak ratios indicated 1) an increase in protein configuration on and surrounding the wound, and 2) increased cellularity that was prolonged in WT mice due to laser treatment. Polarization microscopy confirmed that laser treated WT mice showed increased

heterogeneity in collagen orientation. HSP70 is active in protein configuration and cellularity of early wound healing. Laser preconditioning enhances the effects of HSP70 in ways consistent with findings of previous studies. Raman spectroscopy proved a convenient non-invasive method of obtaining information for evaluating these effects and efficacy of wound healing laser treatment.

1. Introduction:

Wound repair is a complex coordinated sequence of overlapping biochemical and cellular events that result in the restoration of damaged tissue [1]. Under normal conditions of wound repair, the processes that result in healing of injured tissue follow a specific and well-defined time course. Various disorders, including diabetes and burn wounds, create conditions that impair the normal sequence of wound repair [2] causing many patients to eventually develop chronic wounds [3, 4]. High mortality rates and a growing number of limb amputations, roughly 100,000 per year in the US alone from diabetic foot ulcers, have sparked investigation into a variety of novel preventative and treatment strategies for enhancement of wound healing.

In one such method, researchers have shown that pre-treating cells or tissues with an initial mild thermal stimulus (often referred to as preconditioning), elicits a stress response that can serve to protect the tissue from subsequent lethal stresses [5-7]. There is evidence that heat shock proteins (HSP's) are largely responsible for this preconditioning phenomenon. While a variety of tissue heating methods have been used, preconditioning results using laser irradiation have been proven to be most effective due to the uniform and controlled temperatures induced in cells and tissue. Moreover, laser-based approaches provide the ability to induce tissue heating in a non-contact fashion (unlike metal contact probes) which in turn is expected to reduce pain and mitigate the risk for infection. Recent results demonstrate that laser preconditioning tissue 6-12 hours prior to cutaneous injury (scalpel incision and laser ablation) significantly accelerates wound healing yielding greater tensile strength and improved cosmetic outcome [8]. It was shown

that 1) HSP70 upregulation is required for a efficient preconditioning response [9]; and 2) HSP70 is a useful biomarker for therapeutic efficacy of improved wound healing after tissue preconditioning [8]. Using Bioluminescence imaging (BLI), a novel molecular imaging approach, optimization of HSP70 expression was possible. Since the promoter sequence for HSP70 drives expression of optically active reporter genes (luciferase and GFP) in a transgenic mouse, BLI enabled real time quantification of the efficacy of tissue preconditioning *in vivo* without the need to sacrifice the model for histological analysis. By quantifying HSP70 over time, the preconditioning protocol has been optimized for normal tissues prior to wound induction.

While the exact role of HSP70 has not been clearly established, it has been shown that HSP70 expression is correlated with thermal stress and subsequent repair as part of the thermal (pre)conditioning response. In normal wound repair, HSP70 is rapidly induced but in the chronic wound setting, HSP70 is decreased [10]. Thus it is logical to hypothesize that a thermal modulation protocol will elevate basal levels of HSP's and result in accelerated physiologic repair of the chronic wound.

However, in order to translate the preconditioning protocol to a clinically relevant thermal modulation protocol, development of a noninvasive, *in vivo* method that is capable of analyzing tissue biochemistry is of critical importance. Such a technology will be required to optimize laser preconditioning parameters. Raman spectroscopy utilizes the vibrational level energy change of laser light as it scatters off chemical bonds to provide a molecular-specific biochemical fingerprint, the analysis of which can be automated to provide realtime information of the tissue state. Conventional Raman Spectroscopy (RS), as used for in-vivo applications, utilizes a fiber optic probe design in combination with a fast acquisition protocol and automated pre-processing. Such a system could be used for treatment optimization as well as clinical wound healing analysis. Spectral markers allow for optimization of laser treatment effects on the healing wound, while providing tissue level information about the wound itself.

Raman Spectroscopy has been used for decades in the field of analytical chemistry, especially for the examination of pharmaceutical quality [11]. The analysis of purified compounds, molecules, and cultured cells indicated that Raman scattering is sensitive to conformational changes and capable of distinguishing features of biochemical content. Raman spectra of nucleic acids are sensitive to DNA conformational forms, backbone organization, and the relative contributions of specific base pairs, even distinguishing differences in phosphate stretching between DNA and RNA [12].

Developments of near infrared (NIR) laser sources designed for Raman spectroscopy minimize the impact of tissue fluorescence on collection, allowing for feasible application to a wide variety of biomedical problems; however, relatively few have pursued the use of Raman Spectroscopy to tissue applications or *in vivo* studies [13-15]. Several tissues, including arterial tissue [16] and bone [17, 18], make ideal environments for the use of RS as a quantitative measure of disease. Despite the greater challenges posed to the use of RS in heterogeneous soft tissues (broadened spectral features, increase in fluorophore concentration), the use of NIR Raman spectroscopy has led to significant success in the diagnosis of complex diseases including breast and cervical cancer [12, 14, 19-23].

Owing perhaps to accessibility, the study of skin using Raman Spectroscopy is also largely motivated by the numerous debilitating skin diseases that could be properly treated or even cured if diagnosed or assessed early in development. The development of confocal and fiber optic Raman instrumentation represents the potential for real-time surgical guidance, and subsequent decreases in procedure cost and patient recovery time [13, 24]. Raman Spectroscopy has also been used to correlate the putative antioxidant role of skin carotenoids to cancerous lesion prevention [25]. In cosmetic applications, confocal Raman microspectroscopy has been used *in vivo* to demonstrate a depth-dependent distribution of natural moisturizing factor, a well-characterized byproduct of enzymatic degradation to preserve moisture in the stratum corneum in dry environments [24]. The diversity of successful applications of Raman Spectroscopy to skin

supports the hypothesis that Raman Spectroscopy could viably be used for *in vivo* analysis of cutaneous wound healing.

Despite the possibility of a natural extension of ongoing studies in bone or skin, remarkably few research groups have pursued the investigation of wound healing or tissue repair using optical spectroscopies. Zhang et al. utilized the relative strengths of both Infrared (IR) Spectroscopy and confocal Raman spectroscopy to visualize the keratin-rich reepithelialization front and the spatial distribution of elastin and collagen within the wound bed, respectively [26]. Chan et al. analyzed an *ex vivo* human skin wound culture model with IR and confocal Raman spectroscopies over several days. Subsequent deconvolution of confocal mappings using factors with distinct elastin and collagen features allowed for spatial-temporal distribution of major structural proteins [27]. Crane et al. demonstrated qualitative differences between healing and chronic wound spectra from wound biopsies of soldiers [28]. Alimova et al. analyzed the changes in spectral content as a function of incisional wound closure via traditional suture or experimental laser tissue welding from two different lasers at discrete time points in the healing process of four guinea pigs [29]. This work reported in this thesis differs from other reports of spectroscopic wound healing in several ways. The Raman spectroscopy acquisition protocol for this study utilizes irradiances and collection times currently approved for clinical study. Secondly, this work represents the first known report of Raman sensitivity to spectral differences in the healing wound and neighboring tissue as a function of both genetic expression as well as treatment response.

This study seeks to confirm an active role for HSP70 in untreated and laser preconditioned wound healing by detecting *in vivo* differences in downstream biochemistry via Raman spectroscopy. The novelty of this study lies in the clinical and laboratory relevance of the methods, allowing for possible future integration and optimization of subtle laser preconditioning treatments, as well as the investigation and early diagnosis of altered wound healing. Towards achieving these goals, 19 wild-type (WT) and HSP70 knockout (HSP70^{-/-}) C57BL/6 mice underwent normal and laser preconditioned incisional wounds. Daily collection of a spatial

distribution of Raman spectra built a time course for the changes in wound healing progression, while the analysis of peak ratios highlighted the suggested biochemical relevance of these differences due to genetic expression of HSP70 and the response to laser preconditioning treatment. The results of findings via RS were then qualitatively confirmed using standard and polarization microscopy. Ultimately, Raman Spectroscopy achieved a clinically relevant, non-invasive, in-vivo, spatio-temporal biochemical analysis of murine skin incisional wounds as a function of laser preconditioning and the presence of HSP70.

2. Methods:

2.1 Mouse Model and Preparation:

A pre-conditioning and wounding protocol as described below was followed using C57BL/6 mice under the approval of and conducted in accordance with procedures established by the Vanderbilt Institutional Animal Care and Use Committee (IACUC). HSP70 knockout mice were the model described by Hunt et al. [30], acquired through the Mutant Mouse Regional Resource Centers (B6;129S7-Hspa1a/Hspa1b^{tm1Dix}/Mmcd). Nineteen adult female mice, 10 wild-type (WT) and 9 HSP70 knockout (HSP70^{-/-}), were anesthetized with isoflurane. While under anesthesia, dorsal fur was clipped and remaining fur was removed using depilating cream. The affected area was then repeatedly rinsed and wiped down with alcohol wipes to prevent any undesired reaction. Mice were then returned to animal care and observed for 36-48 hours, during which any observation of inflammation, pigmentation in the area to be treated, superficial wounds, or chemical reaction, resulted in exclusion of those animals from the study.

Upon routine inspection no less than 24 hours prior to treatment, the dorsal skin of anesthetized mice was cleaned and disinfected, and target areas were surrounded with a series of manually created tattoos to ensure consistency of location both throughout preconditioning, surgery, and wound healing analysis. Tattoos were placed just below the epidermis using 28 gauge needles with India ink no less than 1 cm away from the target location. To prevent bias due to anatomical variation, contralateral target locations were consistently chosen 1-1.5 cm caudal to the base of the skull and centered 0.8-1cm lateral from the spine. Any improper tattooing or spreading of ink was considered grounds for study exclusion.

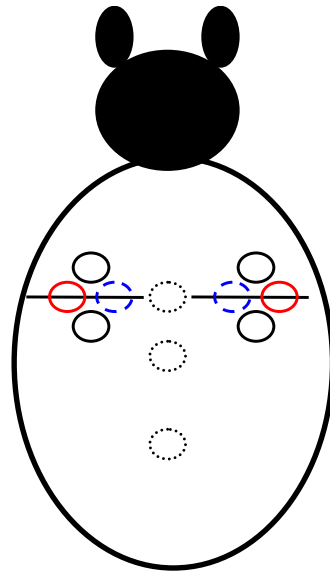


Figure 1. Diagram of mouse model dorsum wound and Raman spectra collection location indicates grouping by anatomical locations and subsequent similar biochemical trends: Intact skin adjacent to wounds (solid black); lateral wound samples (solid red); medial wound samples (dashed blue). Dotted black sample along the spine were used to help establish stability of skin spectra as a function of spatial location and hair regrowth but not directly used in analysis.

2.2 Laser Preconditioning and Surgery:

Twelve hours prior to surgery, anesthetized mice underwent laser preconditioning on one of the two target dorsal locations. Preconditioning location was randomly selected via coin toss. Preconditioning protocol was conducted with an Aculight Renoir diode laser (Renoir; Lockheed Martin Aculight, Bothel, WA) coupled into a 600 μm diameter, multimode silica fiber according to Wilmink et al. ($\lambda=1.85\mu\text{m}$, $H_0=7.64\text{mJ}/\text{cm}^2$, spot diameter=5mm, Rep. rate=50Hz, $\tau_p = 2\text{ms}$, exposure time = 10 minutes) [8]. During laser exposure, tissue temperatures were measured in real time using an infrared camera sensitive to changes of $\pm 0.1^\circ\text{C}$ (A20 series, FLIR Systems, Portland, OR). ThermaCAM Researcher 2.8 was used to record temperature traces and conduct data analysis. In assuring consistency with results from Wilmink et al. [8], generated temperatures were verified to be approximately 43-44.5 $^\circ\text{C}$.

Twelve hours after preconditioning, mice were once again anesthetized with isoflurane. To achieve sterile conditions and prevent the influence of infection, the surgical area was cleansed with povidone-iodine solution and alcohol wipes. Using tattoos as guides, two contralateral 1 cm full-thickness linear incisions were made with a #11 scalpel blade. Immediately after the incision, two 7.5 mm Michelle clips were used to close each end of the wound, ensuring the proper opposition of wound edges. Clips were subsequently removed on post-operative day 5 (POD5).

2.3 Raman Spectroscopy: Acquisition and Processing:

The portable Raman system consists of a mode locked diode laser ($\lambda=785\text{nm}$; Innovative Photonic Solutions, Mammoth Junction, NJ) coupled to a custom fiber optic probe (Emvision, Loxahatchee, FL). This probe consists of a single, central $400\mu\text{m}$ diameter excitation fiber surrounded by 7 equally spaced $300\mu\text{m}$ diameter collection fibers with in-line filtering to reject 785nm . Power output from the central excitation fiber was confirmed at $\sim 80\text{ mW}$ for each scan. Collection fibers were coupled to a $f/1.8$ holographic imaging spectrograph (Kaiser Optical Systems, Inc., Ann Arbor, MI), subsequently dispersing light onto a back-illuminated, deep depletion, thermo-electrically cooled CCD (Model# 920- BRD, Andor Technologies plc., Belfast, UK). Each Raman scan consisted of 3 accumulations of 3 seconds each to ensure maximum signal without saturation.

Spectral calibration and processing were performed according to Robichaux-Viehoever et al. [31]. In brief, calibration for system response was calculated using a neon-argon lamp, naphthalene, and acetaminophen to correct for system wavenumber, laser excitation, and light throughput variations. Noise removal was accomplished by vertical binning of the 7 collection fibers (averaging along the intensity axis); horizontal binning to match the Nyquist limit of system spectral resolution; and finally smoothing via second-order Savitsky-Golay FIR filter. Fluorescence subtraction was accomplished using a modified polynomial fit method in which a fifth-order polynomial was fit to the fluorescence baseline. Subsequent to preprocessing algorithms, spectra were then normalized to mean spectral intensity to account for overall intensity fluctuations. Normalized spectra were analyzed as a function of time and spatial location with regards to the intensity of the most prominent peaks and the relative intensity of their ratios.

To eliminate the influence of anatomical variations in skin, eleven Raman spectra (see Figure 1) were acquired from consistent sites on wounded and adjacent intact skin prior to preconditioning, after surgery, and daily thereafter until mice were culled for histology at days 4,

7, and 10. For peak ratio analyses, samples from intact skin immediately adjacent from the wound were separated from medial wound samples and lateral wound samples. At each of these time points, digital photography was used to document the wounds for future reference.

2.4 Histology:

After euthanasia, the entire dorsum of the mouse was excised and divided into 5 mm wide cross-sections of the wound and adjacent intact skin. Following 24 hour formalin fixation, histological cross-sections of the wounds were stained with Hematoxylin and Eosin (H&E) to visualize cellular organization and collagen deposition. Slides were analyzed using a microscope with a polarizing filter. Under polarized light, newer immature collagen displays less birefringence than its mature organized counterpart. As a qualitative confirmation of Raman spectral analysis, photographs of the histology slides under standard and polarized light were visually examined for inflammatory cell concentration, epidermal thickness, collagen intensity, and collagen orientation

3. Results:

3.1 Establishing normal tissue spectral behavior:

Figure 2 illustrates a representative time course (increasing in vertical axis) of Raman spectra of untreated skin healing from the lateral spot (Figure 1, red) wound, starting prior to surgery, and ending on post-operative day 9 (POD9). The bold baseline indicates several peaks of interest in the intensity normalized Raman spectrum of untreated wild-type mouse skin prior to surgical incision. The greatest intensity differences seen throughout the wound healing time course (**Figure 2** gray bars) also correspond to the most prominent pre-operative (Pre-Op) peak intensities: 1265 cm^{-1} , 1304 cm^{-1} , 1440 cm^{-1} , and 1657 cm^{-1} . The most notable changes in peak intensities relative to Pre-Op skin occurred between POD1 and POD3. The general shape of the spectrum seems to return to the baseline preoperative shape by POD 7 or 8. Examining individual peaks, most of the low wavenumber peaks including 723 cm^{-1} , 964 cm^{-1} , 1083 cm^{-1} , and the doublet from 1265 to 1304 cm^{-1} undergo changes in relative intensity between POD1 and POD3 that then return to Pre-Op intensity by POD7. Interestingly, several peak intensity changes that occur between POD1 and POD3 still remain, or even increase by POD7. Spectra indicate increased differences in the shoulder at 1118 cm^{-1} and peaks at 1440 cm^{-1} , 1657 cm^{-1} , and 1730 cm^{-1} . These results suggest that Raman spectra are sensitive to multiple distinct trends within the course of normal incisional wound healing.

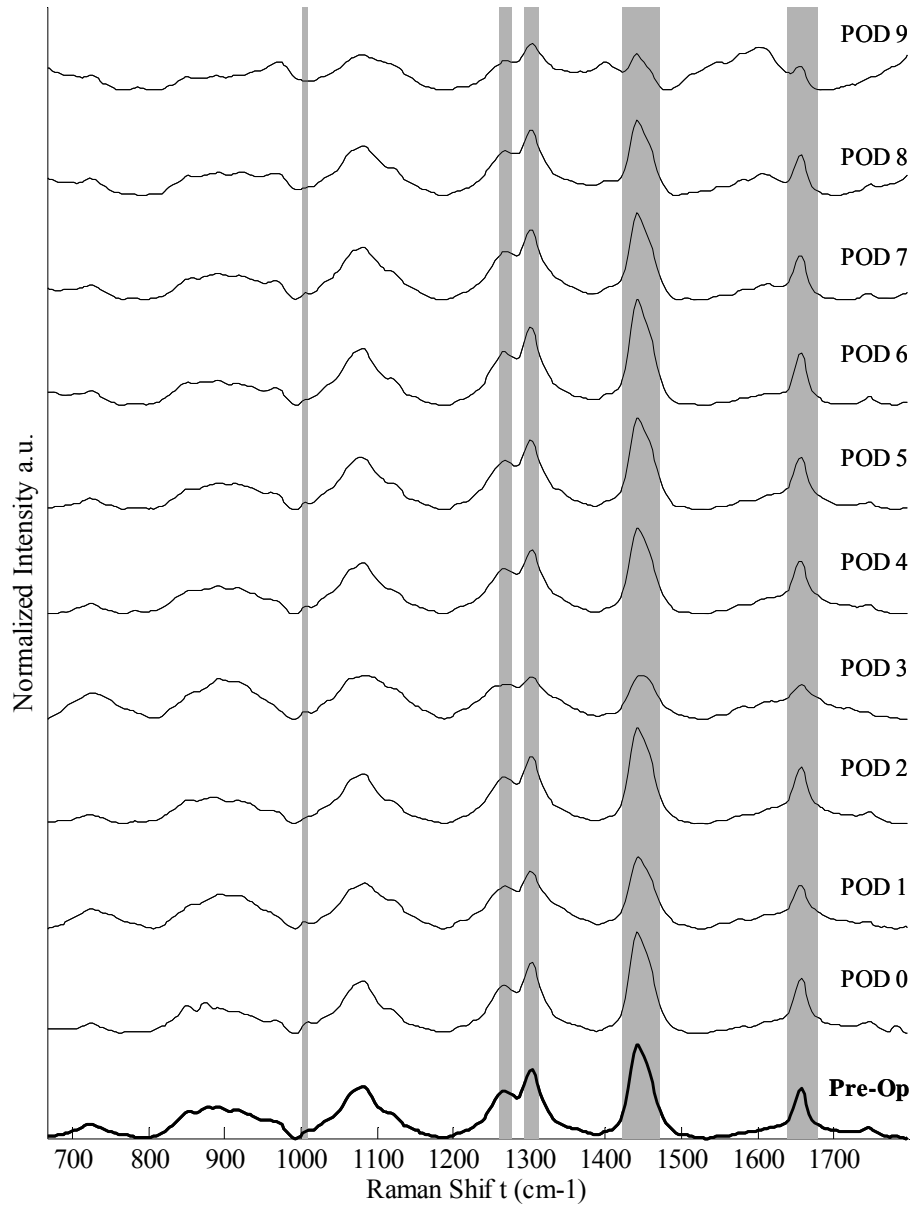


Figure 2. A representative time course of Raman spectra from a single untreated wild-type (WT) lateral wound throughout the wound healing process indicates changes within two days of operation and gradual peak intensity recovery by POD7. Increasing time points (pre-operative, POD 0-7) correlate to increasing y-axis value. Prominent peaks (gray bars) indicate changes throughout the time course at 1265 cm^{-1} , 1304 cm^{-1} , 1440 cm^{-1} , and 1657 cm^{-1} .

Figure 3 provides statistical support for the trends represented in Figure 2. Top panels show mean spectra from untreated wounds in WT mice at POD2 and POD7 relative to Pre-Op spectra. Bottom panels indicate the probability of significant difference between the mean spectra using a paired Student's t-test for each wavenumber. Significance of the t-test is plotted as the probability of rejecting the null hypothesis (mathematically expressed as '1- p ', where p is the probability of accepting the null hypothesis), such that significance increases as the value of '1- p ' approaches 1. This test evaluates the null hypothesis that the intensity of a given wavenumber of Raman shift for a particular post operative day is the same as that of its matching pre-operative spectrum. Peak intensities at 964 cm^{-1} , 1265 cm^{-1} , and 1304 cm^{-1} exhibit statistically significant differences from Pre-Op spectra on POD2; however, on POD7 these peaks no longer show a statistically significant difference from Pre-Op spectra. This indicates a "recovery" of Pre-Op spectral intensity for these peaks. On the contrary, peak intensities at 1118 cm^{-1} , 1440 cm^{-1} , 1657 cm^{-1} , and 1748 cm^{-1} do not exhibit statistically significant differences from Pre-Op spectra on POD2; however, on POD7 these peaks indicate a statistically significant difference from Pre-Op spectra. These findings indicate the development of separate spectral changes beyond POD7.

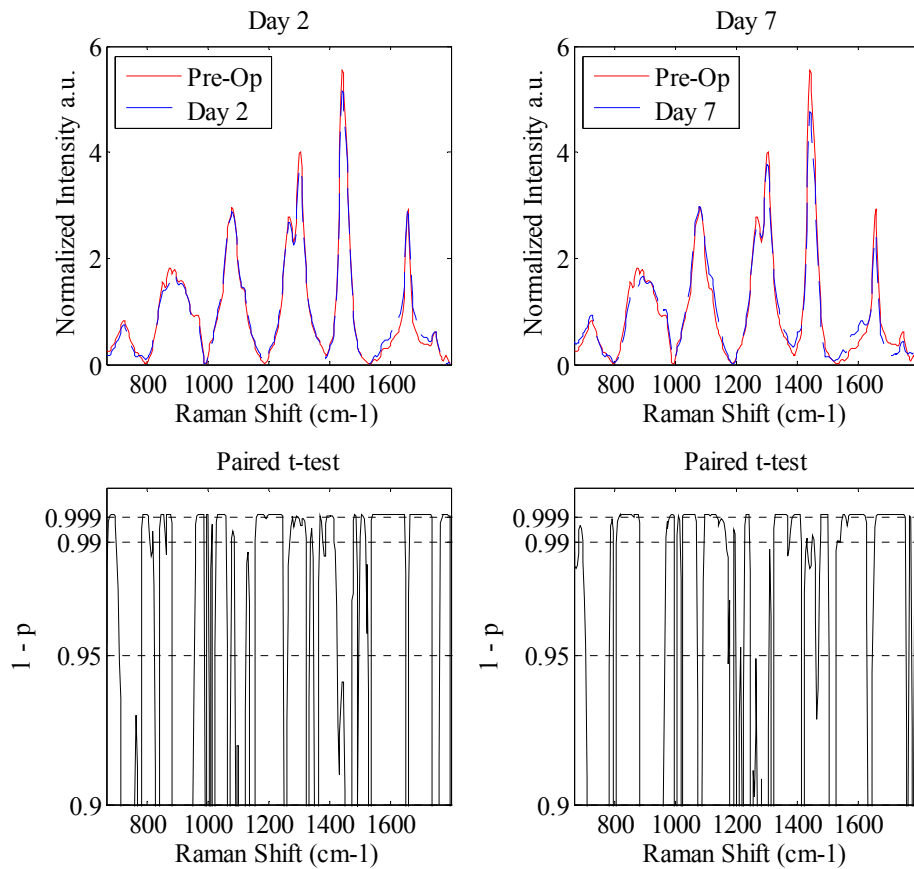


Figure 3. Paired t-tests illustrate recovery or persistence of peak intensity differences of mean spectra on POD2 and POD7 relative to the mean Pre-Op spectrum. Low wavenumber peaks including 726 cm^{-1} , 960 cm^{-1} , 1083 cm^{-1} , 1122 cm^{-1} , and the doublet between 1265 and 1304 cm^{-1} illustrate peak intensity change at POD2 followed by recovery of pre-operative peak intensity by POD7. Peak intensity differences seen in 1440 cm^{-1} , 1657 cm^{-1} , and 1730 cm^{-1} POD2 persist and even increase by POD7.

3.2 Spectral content of preconditioned wounds and effects of HSP70:

Within the time course of untreated wild-type wounds, the period between POD1 and POD3 represents the greatest spectral departure from Pre-Op normal tissue. To examine how these downstream changes are affected by HSP70 genetic expression and laser preconditioning, average spectra from the wound and adjacent skin were constructed for POD2, and two-sample t-tests were conducted to explore the extent and location of spectral changes. Similar in layout to Figure 3, Figure 4 illustrates the downstream effects of HSP70 within treatment groups, in which a point-wise two sample t-test indicates the probability of rejecting the null hypothesis as a function of Raman shift. This test evaluates the null hypothesis that the intensity of a given wavenumber of Raman shift within a wild-type mouse wound is the same as that of an HSP70 knockout wound. HSP70 knockout mice exhibit a significantly stronger spectral intensity through several lower wavenumber bands, including peak intensities at 723 cm^{-1} , 782 cm^{-1} , 898 cm^{-1} , and 964 cm^{-1} . Spectra from HSP70 knockout mice also indicate significantly stronger peak shoulders at 1118 cm^{-1} and around 1657 cm^{-1} . In contrast, wild-type mice exhibit significantly stronger peak intensities at 1083 cm^{-1} , 1265 cm^{-1} , 1304 cm^{-1} , 1440 cm^{-1} , 1657 cm^{-1} , and 1730 cm^{-1} . For both the treated and untreated groups, there is a highly significant difference ($p < 0.001$) between the Raman spectrum on POD2 of a wild-type and HSP70 knockout mouse for all prominent peaks.

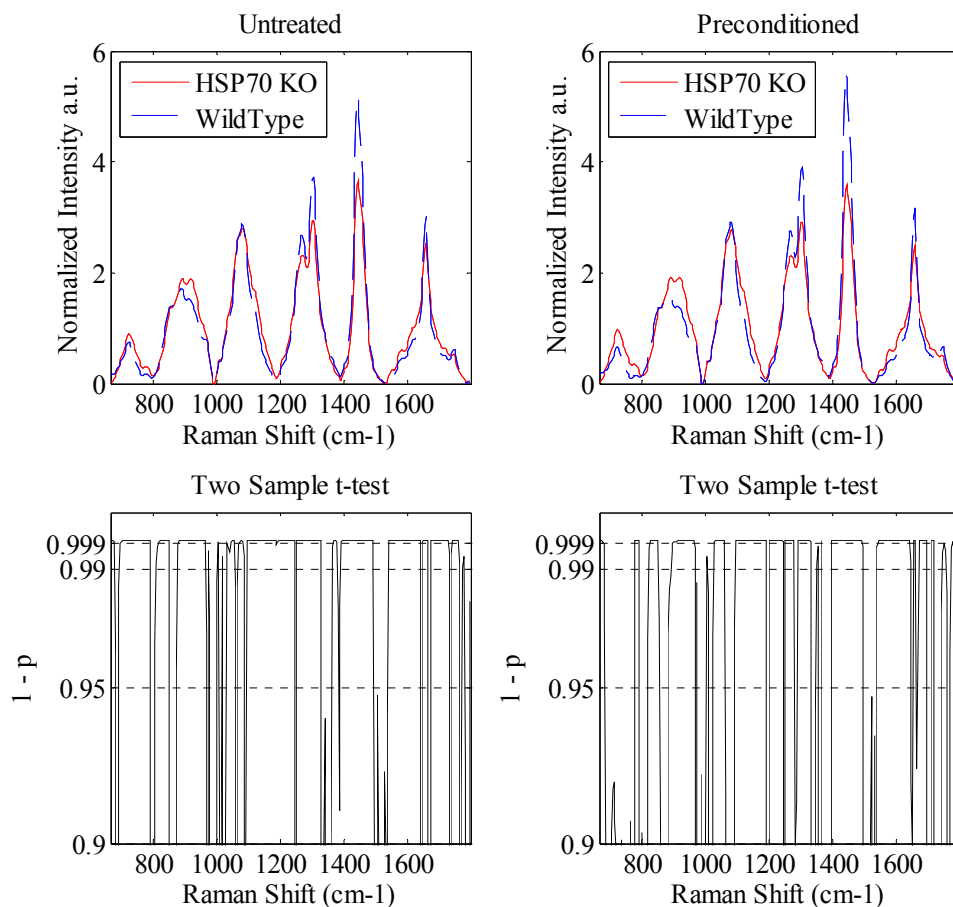


Figure 4. Comparison of average wild-type and HSP70 knockout mouse wound Raman spectra on POD2 indicates significant differences in normalized intensity at peaks of biological interest. Similar spectra results are found for preconditioned wounds on left as those seen for untreated wounds on right, indicating native difference in wound healing due to HSP70 activity.

Figure 5 illustrates the relative effect of the preconditioning upon mean POD2 Raman spectra within genetic mouse type. Laser preconditioning creates numerous differences in the Raman spectra of wild-type mouse wounds, but not in those of the HSP70 knockout mice. In wild-type wounds, significant differences were seen between the intensity of untreated and preconditioned peaks at 723 cm^{-1} and 1083 cm^{-1} . Comparing preconditioned wounds to their untreated counterparts, marginally significant differences (significant at $\alpha = .10$) in the peaks of wounds in wild-type mice were seen at 1118 cm^{-1} , 1265 cm^{-1} , 1304 cm^{-1} , 1440 cm^{-1} , and 1657 cm^{-1} . Statistical significance was also observed as a function of laser preconditioning in wild-type mice through the shoulders of peaks including the valley between 1265 cm^{-1} and 1304 cm^{-1} (at 1285 cm^{-1}), 1440 cm^{-1} (between 1465 and 1475 cm^{-1}), and 1657 cm^{-1} (at 1650 cm^{-1} , 1703 cm^{-1} , and 1730 cm^{-1}). Within HSP70 knockout mice, statistical significant differences in spectra are observed only in the shoulders of peaks at 1083 cm^{-1} (at 1052 cm^{-1}) and 1440 cm^{-1} (at 1489 cm^{-1}). Ultimately, preconditioning induced marginally significant differences in the intensity of prominent Raman peaks of the normal wound healing time course (see Figure 2), but only in wild-type wounds.

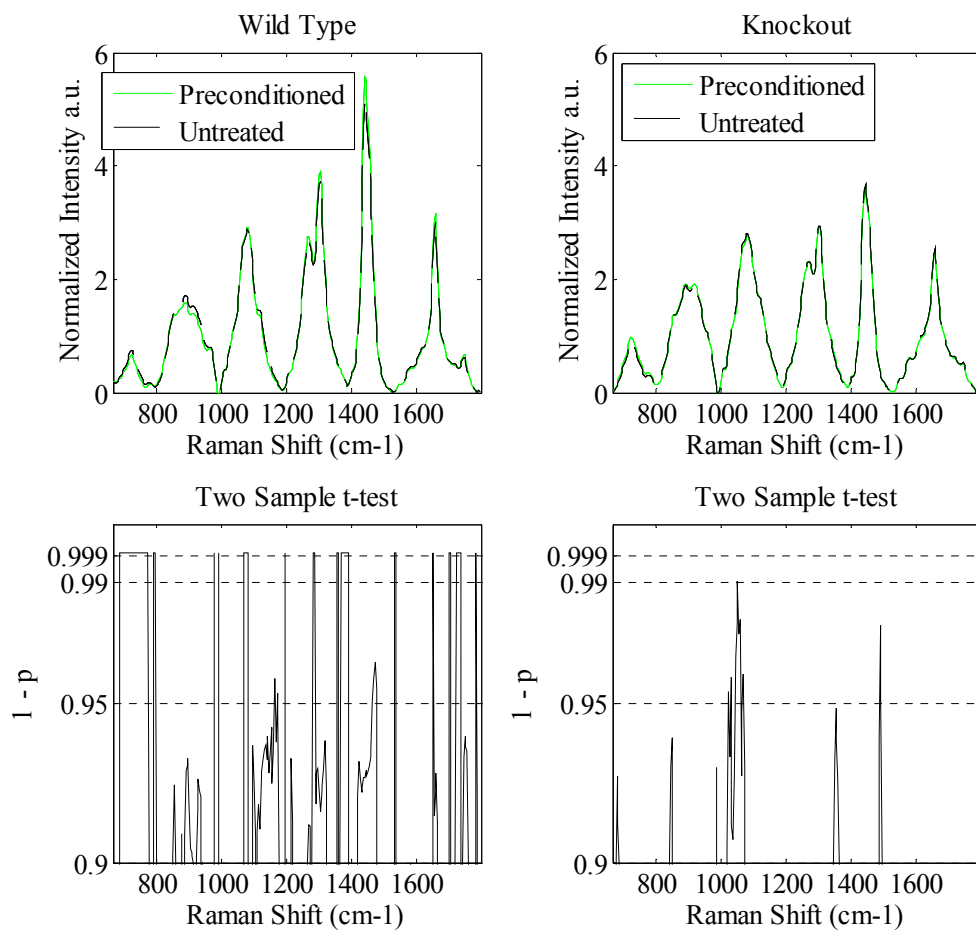


Figure 5. Comparison of average preconditioned and untreated wound Raman spectra on day 2 indicates few significant differences in normalized intensity at peaks of biological interest for wild type samples on left, and no significant differences at peak locations for HSP70 knockout sample on right, suggesting that preconditioning requires HSP70 seen in wild type wounds.

3.3 Peak ratios elucidate the combined effects of HSP70 and preconditioning:

While the analyses shown in Figures 2-5 were limited to absolute peak intensity, peak ratios examine relative intensity differences, allowing for a further analysis of specific spectral changes. For these analyses, Raman spectra were grouped by sample location to prevent the confounding effects of natural anatomical variation in skin (see Figure 1). Figure 6 illustrates the ratio of the normalized peaks at 1440 cm^{-1} to 1657 cm^{-1} with error bars (2 standard deviations in each direction) as a function of time for lateral wound samples (Figure 1, red). Within the context of wound healing, this ratio likely suggests the degree and quality of protein deposition and organization. The trend in ratio peak intensity is similar for both wild-type and HSP70 knockout wounds, exhibiting a decrease until POD3 and a subsequent recovery and even increase by POD7. This agrees with the trends exhibited in Figures 2 and 3. In comparing wild-type versus HSP70 knockout models, statistically significant differences (two sample t-test; $p < .01$) can be seen up to and including POD7. This trend is exhibited in both laser preconditioned (upper right panel) and untreated (lower left panel) wounds. Examination of the time course for this peak ratio yields similar significant trends (not shown) for medial wound spectra (Figure 1, dotted blue) and neighboring intact tissue (Figure 1, black).

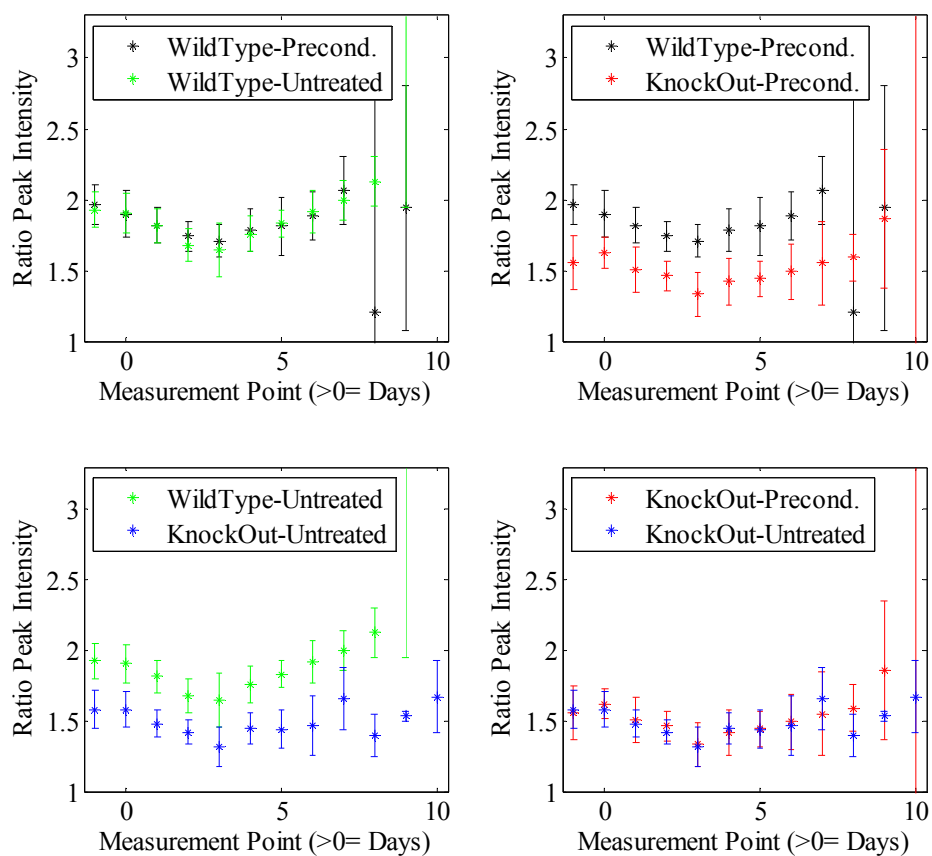


Figure 6. Paired comparisons of time course (POD) of average peak ratio intensity of 1440:1657cm⁻¹ in lateral wound samples indicates significant differences between wounds in wild-type and HSP70 knockout mice for the first 6 days. No significant differences are seen in either wild type or HSP70 knockout as a function of preconditioning. Error bars represent 2 standard deviations (separation indicates p < 0.05). Trends suggest that HSP70 expression correlates to persistent downstream differences in wound healing.

Figure 7 shows the normalized peak ratio of 1304 cm^{-1} to 1265 cm^{-1} over time, indicating a significant difference (two sample t-test; $p < 0.05$) between the early wound healing processes in wild-type mice and those lacking HSP70. This ratio suggests a measure of either cellularity or cellular activity. The trend for both wild-type wounds and HSP70 knockout wounds indicates an initial increase in the ratio peak intensity at POD0, followed by a return to Pre-Op value (POD= - 1) by POD 3 or 4, and a subsequent ratio decay beyond POD4. In untreated wounds this difference is statistically significant ($p < 0.05$) from Pre-Op until POD1; however, laser preconditioning of wild-type mouse wounds amplified this difference on both POD1 and POD2 (compare lower left to upper right panel). Moreover, laser preconditioned wounds exhibit a significant difference in peak ratio between wild-type and HSP70 knockout mouse wounds from Pre-Op spectra up to and including POD5 (top right panel). This suggests that laser preconditioning extends the downstream biochemical effects of HSP70 expression for up to 3 days. Ultimately, this preliminary analysis of peak ratios delineates the time course of specific differences seen as a function of HSP70 genetic expression as well as laser preconditioning.

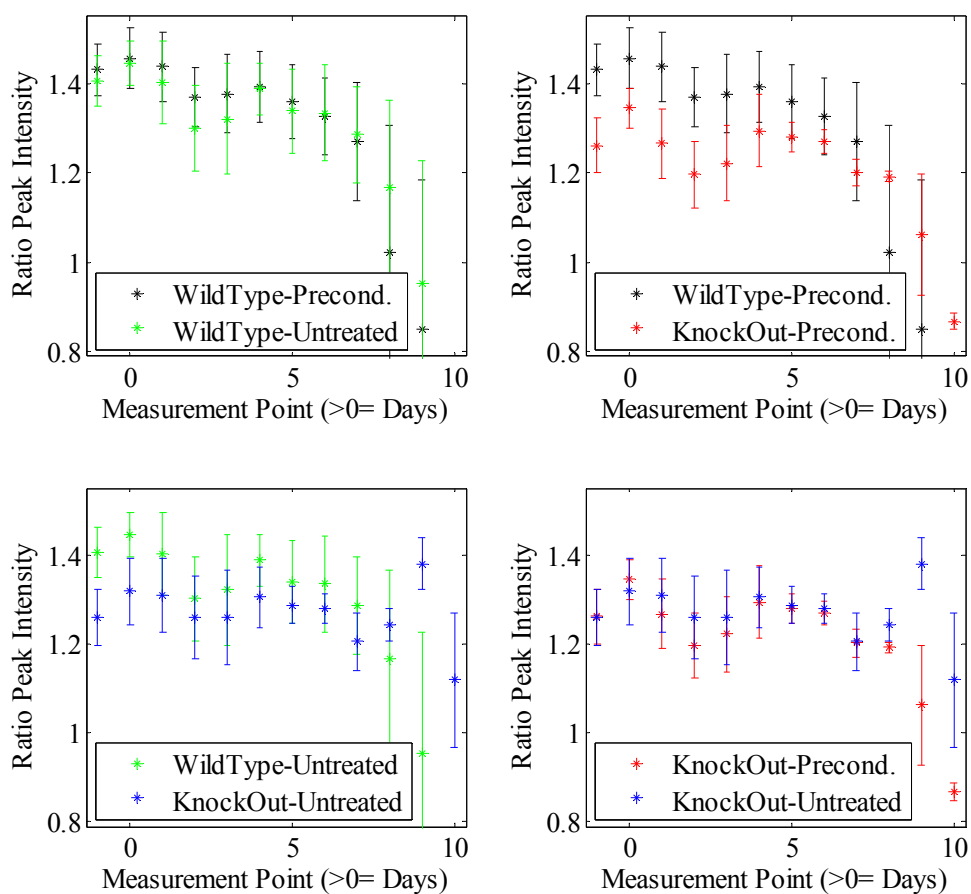


Figure 7. Paired comparisons of time course (POD) of average peak ratio intensity of 1304:1265cm⁻¹ in lateral wound samples indicates significant differences between wild type and HSP70 knockout mice prior to and following surgery. Preconditioning prolongs significant differences between wild type and HSP70 knockout beyond POD1. Error bars represent 2 standard deviations (separation indicates p<0.05). Trends suggest preconditioning prolongs the increase in ratio caused by HSP70, consistent with reported upregulation.

3.4 Histology confirms collagen organization:

Standard microscopic analysis of H&E stained wound cross-sections established the wound healing time course. Separate readings from two expert pathologists agreed that the most prominent healing features occurred prior to POD4; that the wounds were largely reepithelialized by POD7; and most wounds were remodeling on POD10. Slides exhibited no difference in adjacent normal epidermal thickness between wounds in wild-type and HSP70 knockout mice. POD4 histological slides indicated that acute cellular infiltrates from initial inflammation were largely gone, and the wound environment was dominated by macrophages. Histological samples from POD7 indicated complete wound reepithelialization with little residual fibroplasia.

Qualitative histological analysis using polarization microscopy on POD4 and POD7 was utilized to confirm results from Raman spectroscopy. To prevent bias from natural variation between animals, analysis was conducted comparing preconditioned and untreated samples from the same mouse. Figure 8 illustrates the trends seen on POD4. Healing wounds in wild-type mice show less collagen in the wound bed than HSP70 knockout counterparts; however, the organizational patterns of collagen are distinctly more heterogeneous in wounds of wild-type mice compared to HSP70 knockout mice. Both wild-type and HSP70 knockout preconditioned wounds show slightly more total collagen within the wound bed than their untreated counterparts. Figure 9 indicates the downstream results of HSP70 genetic expression and laser preconditioning treatment by examining differences on POD7. Preconditioned wounds of both wild-type and HSP70 knockout mice indicate more heterogeneity of collagen adjoining the repairing wound bed, relative to untreated counterparts. Untreated wounds demonstrate bright collagen birefringence; however, the fibers contributing to this birefringence intensity exhibit a strongly unidirectional distribution. Photographs in figures 8 and 9 are paired representative images that illustrate cumulative trends in qualitative analysis.

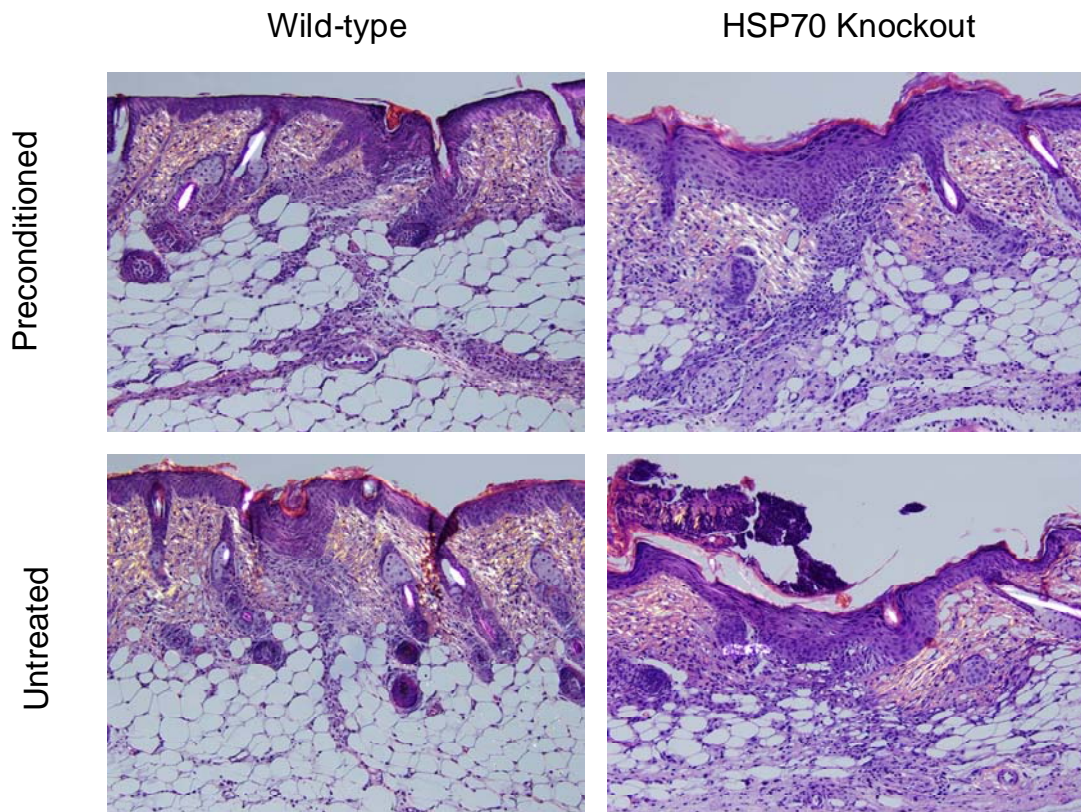


Figure 8. Polarized microscopy of H&E stained wound cross-sections at POD4 indicate increased quantity and directionality of striated collagen in samples from HSP70 knockout mice (right) regardless of pretreatment. Samples from WT mice show relatively less deposited collagen in the wound bed with a more heterogeneous directionality.

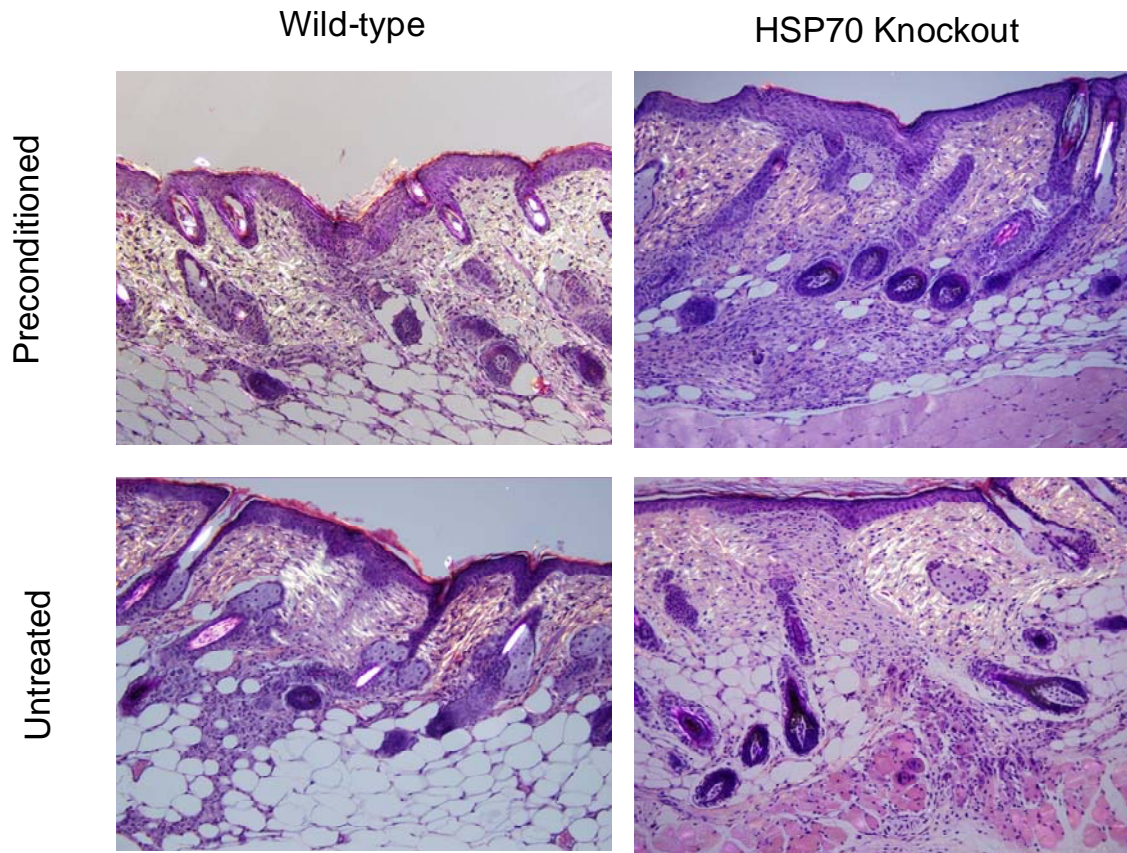


Figure 9. Polarized microscopy of H&E stained wound cross-sections at POD7 indicate directional striated collagen in samples from HSP70 knockout mice (right) and untreated wild type mice (lower left). Preconditioned samples (above) show more heterogeneous directionality than their untreated counterparts (below). Trends suggest that continued heterogeneous matrix replacement is prolonged by preconditioning, consistent with reported increased tensile strength.

4. Discussion:

The use of probe-based Raman spectroscopy (RS) represents a novel method of real-time, *in vivo*, quantitative analysis of wound healing. In what we believe to be the first report of the impact of differential genetic expression on wound healing using Raman Spectroscopy, this method was sufficiently sensitive to resolve the downstream tissue-level impact of HSP70 upon incisional wound healing. Moreover, the analysis of relative peak intensities in the Raman spectra delineated the time course effects of differential wound healing treatment response through non-invasive, *in vivo* measurements. In our studies, RS represents a plausible method for future optimization and tracking of laser preconditioning towards clinical applications. The success of RS in this study also implies many applications in the investigation of future wound healing therapies. As a non-invasive technique to quantitatively probe tissue biochemistry, Raman Spectroscopy is especially promising for the evaluation of nascent wound healing therapies due to its applicability to both laboratory and clinical studies. Finally, the detection of differences in the wound healing time course of HSP70 knockout mice supports the future investigation of RS as a method for the differential diagnosis of altered or chronic wound healing. This avenue of investigation will also be furthered by recent advances in the automated classification of Raman spectra for cancer diagnosis [20].

4.1 Characterizing normal incisional wound healing

In order to characterize tissue biochemistry modulation during wound healing with therapeutic intervention, changes were evaluated relative to the normal state of local tissue. The

time course of wild-type incisional wound healing seen in Figure 2 exhibits distinct trends within the first week of healing. Prominent peaks at both 1265 cm^{-1} and 1304 cm^{-1} change intensity relative to pre-operative spectra, yet recover normal intensity by POD7; however, the later changes seen in the peak intensities at 1440 cm^{-1} and 1657 cm^{-1} are amplified beyond POD7. Taken together with support from Figure 3 paired t-tests, trends in the significant differences may imply a spectral profile for known wound healing phases. In murine wound healing, the changes seen between POD1 and POD3 would likely correspond to the inflammatory phase of wound healing, supported by the histological observation of the absence of acute inflammatory cells by POD4. Moreover, the spectral results seen at and beyond POD7 would correlate to early remodeling phase of murine wound healing, supported by the histological observation of complete reepithelialization by POD7. While the correlation of spectral changes to the observed histological time course shows promise for the use of RS, a more detailed analysis is necessary before a spectral profile of specific wound healing phases can be established within the continuity of the wound healing process.

Using tissue Raman literature, preliminary peak assignments have been made for the prominent peaks shown in Figure 2 to further illustrate the relevance of Raman spectral components in light of known wound healing parameters. Both 1265 cm^{-1} and 1304 cm^{-1} are associated specifically with the amide III (C-N stretch, N-H in-plane bend) bond of a protein in α -helix configuration; however, while the former is more often correlated to structural proteins, the latter falls on the edge of the range associated with nucleic acids and histones, proteins involved in the packaging of DNA [12]. The peak at 1304 cm^{-1} has also been associated with the CH_2 twisting of lipids [32, 33], specifically the phospholipid membrane [23]. Regardless, both of these assignments correlate with cellularity and cellular activity. A Raman shift of 1440 cm^{-1} is associated with the CH_2 stretch of protein side chains, and is most often associated with the quantity of structural proteins in tissue [12]. While the peak intensity of the CH_2 stretch at 1440

cm^{-1} likely has some contribution from the bonds found in lipids, the large degree of temporal change seen in this peak supports the assignment to protein side chains in the context of wound healing. The peak at 1657 cm^{-1} relates to the Amide I bond, and subsequently to the conformation and secondary structure of proteins. As an aside, mouse skin exhibits a notable lack of the distinct phenylalanine peak (1006 cm^{-1}) seen in human skin samples.

4.2 Spectral content implies HSP70 role in wound healing and laser preconditioning:

Given the suggested significance of the strongest spectral components in murine skin, further analysis of the effects of laser preconditioning required an understanding of how these spectral components vary in the course of wound healing, especially as a function of the presence or absence of HSP70. Figure 4 suggests that HSP70 plays an active role in the early stages of the wound healing process, although the results do not identify the precise mechanism. Note that the differences in peak intensity throughout the spectrum are seen regardless of laser preconditioning. Furthermore, the involvement of all prominent spectral peak intensities suggests the involvement of HSP70 in both cellular and acellular components crucial to normal repair. The wide variety of biochemical changes illustrated by peak intensity differences is supported by the ubiquity of HSP70, as well as its numerous roles in protein folding, re-folding, and apoptotic pathway suppression [34, 35].

Beyond the involvement of HSP70 in normal wound healing, Raman spectroscopy suggests that the presence of HSP70 is directly involved with the downstream effects of laser preconditioning. Differences seen in the peak intensities of wounds in wild-type but not HSP70 knockout mice as a function of preconditioning (Figure 5) supports the hypothesis that HSP70 upregulation is necessary to affect the known treatment response to laser preconditioning. While the correlation of HSP70 upregulation to downstream preconditioning effects had been well established [8, 9, 36, 37], the differential effects of the presence of HSP70 expression on the laser

preconditioning therapy have not been quantified otherwise. Only marginal statistical significance (significant at $\alpha = .10$) was seen in prominent peaks as a function of laser preconditioning. It is possible that this study was not sufficiently powered to detect significance in the small changes of absolute peak intensity. Furthermore, this analysis averaged spatially independent samples, including the confounding factors of skin biochemical and anatomic variation. Finally, results found by Wilmink et al. were examined at later time points, suggesting that analysis at any single time point early in the wound healing process might not be sufficient to capture any accumulated developments.

4.3 Mouse model and experimental limitations:

The extent and degree of experimental analysis was limited largely by the use of a mouse model. The model represents the only available HSP70 knockout, chosen for the ability to exercise a controlled examination of the role of HSP70 in normal and laser preconditioned wound healing. Unfortunately, it was not possible to analyze the combined effects of HSP70 and preconditioning using Raman spectra during the remodeling phase of wound healing (>7 days). Currently, the mouse model of HSP70 knockout mice is only available on the C57BL/6 background, which is known to develop abnormal skin pigment after around 10 days in response to even mild abrasion.

A brief pilot study (data not shown) indicated that this pigmentation was not the result of either laser preconditioning or depilation. Simple trimming of dorsal hair was sufficient to cause hyper-pigmentation during hair regrowth under normal mouse model activity. The development of this severe hyper-pigmentation significantly changes tissue optical properties and leads to peaks in the Raman fingerprint region that obfuscate analysis. Despite efforts to recover Raman spectra, the development of pigment (observed beyond POD8) makes Raman analysis of the remodeling phase of wound healing intractable with this animal model. The presence of pigment,

coupled with low sample numbers beyond POD7, is responsible for the large error bars seen in Figures 6 and 7, as well as the gross changes in spectral shape in Figure 2 on POD8 and POD9. The data was included to demonstrate this limitation of the model for future reference and also because some mice did not develop pigmentation and the beginnings of remodeling trends offer a more comprehensive shape to the peak ratios relative to expected wound healing time course. These model limitations further prevent the spectral confirmation of long-term preconditioning effects reported by Wilmink et al. [8]; however, the model was sufficient to confirm the active role of HSP70 and provide some insight into biochemical response to laser preconditioning due to HSP70 upregulation.

4.4 Significance of peak ratios through the wound healing time course:

Eliminating confounding factors seen in the comparison of absolute wavenumber intensity, peak ratios isolated to particular anatomical locations allowed for further analysis of specific changes over time. The ratio of peaks at 1440 cm^{-1} to 1657 cm^{-1} compares the CH_2 stretch of proteins, found in protein side chains, to the presence of the Amide I bond, found near amino acid residue linkages. As a ratio, these wavenumbers yield information regarding the degree of conformation and organization of proteins relative to their quantity. Within the context of wound healing, this ratio likely suggests the degree and quality of protein deposition and organization. Recall the functions of HSP70 as a chaperone during protein folding and repair [35]. Results by Wilmink et al. indicate decreased scarring and increased maximum tensile load of wounded skin samples as a function of HSP70 upregulation on POD7 and POD10, implying increased deposition and organization of structural proteins due to HSP70 activity [8]. Consistent with these results, the significant difference of ratio peak intensity between wild-type and HSP70 knockout mice throughout the first week of healing supports the hypothesis that HSP70 is actively involved in the deposition and repair of structural proteins in the extracellular matrix.

Finally, the observations of similar significant trends from other wound spatial locations and adjacent intact skin implies the collection of wound spectral characteristics from the edge of the wound bed, mitigating possible future confounding factors in more complex wound environments.

The ratio of peaks at 1304 cm^{-1} to 1265 cm^{-1} compares specific amide III bonds of proteins in α -helix configuration. The 1265 cm^{-1} intensity is more often correlated to structural proteins, while the 1304 cm^{-1} is associated with both histones and nucleic acids, and subsequently net nuclear material [12]. By differentiating between neighboring peaks both associated with the amide III bond, the ratio suggests a measure of either cellularity or cellular activity. Note that the alternative assignment of 1304 cm^{-1} to the CH_2 twisting [32, 33] in phospholipid membranes [23], yields a ratio with similar implications on cellularity or cellular activity. Because the 1265 cm^{-1} intensity alone does not discriminate between extracellular or intracellular protein, further studies would be needed to narrow these observations towards either cellularity or cellular activity.

Significant differences were observed in ratio peak intensity between wounds in wild-type and HSP70 knockout mice prior to POD2, regardless of laser preconditioning. This implies that HSP70 activity has a direct effect on cellularity during the early phases of wound healing, possibly through its known suppression of apoptotic signaling pathways. Moreover, laser preconditioning protocol led to an increase of this elevated cellular trend by at least two days. It is important to note the time range of these results. Increased cellularity occurring within the wound closure and inflammation phases as seen in Figure 8 may lead to a decrease in total healing time and increased tissue organization. Recall that histological observations indicated a lack of acute inflammatory infiltrates and the presence of reepithelialization on POD4. This trend fades appropriately as the reepithelialization phase of wound healing makes way for the remodeling phases, during which any increased cellularity would be seen as a negative impact, prolonging the wound healing process.

4.5 Histology confirms RS trends for HSP70 and laser preconditioning

While qualitative histological analysis establishes some boundaries for wound healing phases relative to observed spectral differences, the result implies limited applicability of semi-quantitative analysis of healing features at these precise timepoints. The incisional wound model and histological timepoints were chosen to mimic the experimental protocol of Wilmink et al. while providing optimal environment for Raman measurements; however, incisional wounds provide little volume for quantitative histology. Nevertheless, the lack of acute cellular infiltrates on POD4, as shown in Figure 8, supports peak ratio results for cellularity (1304 cm^{-1} to 1265 cm^{-1}) in which the greatest difference as function of preconditioning was seen on POD2.

Polarization microscopy was used to confirm the relative protein conformation and organization seen in the peak ratio of 1440 cm^{-1} to 1657 cm^{-1} . Collagen birefringence intensity correlates to maturity, and the directionality of birefringent fibers is indicative of organizational heterogeneity and indirectly, the degree of crosslinking. This can be seen macroscopically in scar tissue as large scale striation patterns. Results from Wilmink et al. [8] indicate that optimization of preconditioning based on maximal HSP70 upregulation indicated increased tensile strength and cosmetic appearance, both indicative of structural protein content and organization.

The lower quantity and greater heterogeneity of wild-type wound bed collagen suggested by Figure 8 may indicate that the intra-cellular protein-folding role of HSP70 indirectly influences the subsequent organization of collagen incorporation into the extracellular matrix. This would both confirm results by Wilmink et al. as well as support Raman spectra results from the 1440 cm^{-1} to 1657 cm^{-1} peak ratio (Figure 8). The relative increase in collagen heterogeneity seen in both wild-type and preconditioned wounds on POD7 (Figure 9), when examined in reference to POD4 observations, indicates that preconditioning may have some effect on other active wound healing proteins independent of HSP70. However, the heterogeneity is more pronounced in wild-type wounds, consistent with the chaperone protein activity associated with HSP70 as well as the results seen from the peak ratio of 1440 cm^{-1} to 1657 cm^{-1} .

Untreated wounds demonstrate bright collagen birefringence on POD7, indicative of collagen maturity; however, the strongly unidirectional distribution of the collagen indicates less organization and the potential for greater scarring. While quantitative analysis of both directionality and intensity were possible, it is important to note that hair follicle regrowth could have drastically skewed results. The presence of hair follicles, while indicative of high quality healing, also manifests as striations in collagen when the histological section is shallow of the follicular cross section. Therefore semi-quantitative analyses would either have included automated error or human bias. Reported trends were the result of careful analysis of serial histological samples to exclude the influence of hair follicles on collagen organization. Subsequently photographs in figures 8 and 9 are paired representative images that illustrate cumulative trends in qualitative analysis.

4. Conclusions and Future Directions:

Raman spectral analysis is consistent with the hypothesis that HSP70 plays an active intracellular role in subsequent collagen deposition and matrix organization during the early stages of wound healing. This finding is consistent with the HSP family role as chaperone proteins responsible for the refolding and repair of damaged protein. It is important to recall that HSP70 is believed to be an intracellular protein, yet its expression will have an indirect effect on the extracellular matrix proteins that are produced within cells in the wound bed. Moreover, Raman spectra delineated significant differences in gross biochemical content between wounds in wild-type and HSP70 knockout mice. Preconditioning had its greatest effects on biochemical content in early stages of wound healing. Moreover, differences seen in the spectral intensity distribution of wounds in WT mice were more significant than those in HSP70 knockout mice, suggesting that preconditioning amplifies natural HSP70 effects via upregulation.

Peak ratio analysis indicated that HSP70 function during wound healing significantly affects protein conformation and organization prior to remodeling. Moreover, HSP70 was found to be responsible for increased cellularity in the first few days of wound healing, and preconditioning extended this effect, accelerating the natural phases of wound healing. Polarization microscopy confirmed the impact of HSP70 and preconditioning on the downstream organization of collagen in wound extracellular matrix.

Despite study limitations due to animal model physiology and availability, Raman spectroscopy proved an invaluable modality for the assignment of pseudo biomarkers for a detailed analysis of the role of HSP70 in wound healing and its relationship with preconditioning therapy. Its non-invasive nature allowed for the collection of a complete spatio-temporal distribution of biochemical content throughout the wound healing process; subsequently yielding statistically significant results of a multivariate data set with only 38 wounds. To the best of our knowledge, this paper represents the first *in vivo* Raman spectroscopy analysis of the wound healing time course as a function of model genetic expression and treatment. It is important to note that none of the instrumentation, processing algorithms, or peak assignments have been thoroughly optimized for wound healing biology. Thus the full potential of Raman spectroscopy has yet to be realized for either the analysis of wound healing therapeutic efficacy or differential diagnosis. Current efforts include closed-loop automated spectral processing and classification algorithms for wound healing diagnosis. Nevertheless, the spectral dataset confirms that the laser preconditioning protocol effects are a direct result of HSP70 upregulation. Furthermore, Raman spectroscopy will be an analytical tool capable of assessing optimization of future conditioning protocols during translation of laser thermal modulation to clinically relevant skin models and chronic wound scenarios.

Works Cited

1. Davidson, J.M. and S.I. Benn, *Biochemical and molecular regulation of angiogenesis and wound repair*. In: Cellular and Molecular Pathogenesis, A.E. Sirica (ed), Raven Press, New York, 1996: p. 79-108.
2. Braddock, M., C.J. Campbell, and D. Zuder, *Current therapies for wound healing: electrical stimulation, biological therapeutics, and the potential for gene therapy*. Int J Dermatol, 1999. **38**(11): p. 808-17.
3. Harris, M.I., et al., *Prevalence of diabetes, impaired fasting glucose, and impaired glucose tolerance in U.S. adults. The Third National Health and Nutrition Examination Survey, 1988-1994*. Diabetes Care, 1998. **21**(4): p. 518-24.
4. Frykberg, R.G., *Epidemiology of the diabetic foot: ulcerations and amputations*. Adv Wound Care, 1999. **12**(3): p. 139-41.
5. Li, Y., et al., *Retinal preconditioning and the induction of heat-shock protein 27*. Invest Ophthalmol Vis Sci, 2003. **44**(3): p. 1299-304.
6. Kim, J.M., et al., *Effect of thermal preconditioning before excimer laser photoablation*. J Korean Med Sci, 2004. **19**(3): p. 437-46.
7. Topping, A., et al., *Successful reduction in skin damage resulting from exposure to the normal-mode ruby laser in an animal model*. British Journal of Plastic Surgery, 2001. **54**(2): p. 144-150.
8. Wilmink, G.J., et al., *Molecular imaging-assisted optimization of hsp70 expression during laser-induced thermal preconditioning for wound repair enhancement*. J Invest Dermatol, 2009. **129**(1): p. 205-16.
9. Beckham, J.T., et al., *Role of HSP70 in cellular thermotolerance*. Lasers Surg Med, 2008. **40**(10): p. 704-15.
10. McMurtry, A.L., et al., *Expression of HSP70 in healing wounds of diabetic and nondiabetic mice*. J Surg Res, 1999. **86**(1): p. 36-41.
11. Matousek, P., *Deep non-invasive Raman spectroscopy of living tissue and powders*. Chem Soc Rev, 2007. **36**(8): p. 1292-304.
12. Mahadevan-Jansen, A. and R.R. Richards-Kortum, *Raman spectroscopy for the detection of cancers and precancers*. Journal of Biomedical Optics, 1996. **1**(1): p. 31-70.
13. Nijssen, A., et al., *Towards oncological application of Raman spectroscopy*. J Biophotonics, 2009. **2**(1-2): p. 29-36.
14. Kanter, E.M., et al., *Application of Raman spectroscopy for cervical dysplasia diagnosis*. J Biophotonics, 2009. **2**(1-2): p. 81-90.
15. Hanlon, E.B., et al., *Prospects for in vivo Raman spectroscopy*. Phys Med Biol, 2000. **45**(2): p. R1-59.
16. Romer, T.J., et al., *Histopathology of human coronary atherosclerosis by quantifying its chemical composition with Raman spectroscopy*. Circulation, 1998. **97**(9): p. 878-85.
17. Bi, X., et al. *Raman spectroscopy for assessment of bone quality in MMP-2 knockout mice*. in *Optics in Bone Biology and Diagnostics*. 2009. San Jose, CA, USA: SPIE.
18. Carden, A. and M.D. Morris, *Application of vibrational spectroscopy to the study of mineralized tissues (review)*. Journal of Biomedical Optics, 2000. **5**(3): p. 259-268.
19. Kanter, E.M., et al., *Effect of hormonal variation on Raman spectra for cervical disease detection*. Am J Obstet Gynecol, 2009. **200**(5): p. 512 e1-5.
20. Kanter, E.M., et al., *Multiclass discrimination of cervical precancers using Raman spectroscopy*. Journal of Raman Spectroscopy, 2009. **40**(2): p. 205-211.
21. Keller, M.D., et al., *Detecting temporal and spatial effects of epithelial cancers with Raman spectroscopy*. Dis Markers, 2008. **25**(6): p. 323-37.

22. Majumder, S.K., et al., *Comparison of autofluorescence, diffuse reflectance, and Raman spectroscopy for breast tissue discrimination*. J Biomed Opt, 2008. **13**(5): p. 054009.
23. Mahadevan-Jansen, A., et al., *Near-infrared Raman spectroscopy for in vitro detection of cervical precancers*. Photochem Photobiol, 1998. **68**(1): p. 123-32.
24. Caspers, P.J., et al., *In Vivo Confocal Raman Microspectroscopy of the Skin: Noninvasive Determination of Molecular Concentration Profiles*. Journal of Investigative Dermatology, 2001. **116**(3): p. 434-442.
25. Darvin, M.E., et al., *Influence of IR radiation on the carotenoid content in human skin*. Optics and Spectroscopy, 2009. **107**(6): p. 917-920.
26. Zhang, G., et al., *Parallel studies of cutaneous wound healing: IR imaging, confocal Raman microscopy, and molecular biology*. Journal of Investigative Dermatology, 2009. **129**: p. 40.
27. Chan, K.L.A., et al., *A coordinated approach to cutaneous wound healing: vibrational microscopy and molecular biology*. Journal of Cellular and Molecular Medicine, 2008. **12**(5B): p. 2145-2154.
28. Crane, N.J., et al. *Raman Spectroscopic Analysis of Warrior Wound Biopsies: What Happens When Good Wounds Go Bad?* in *The Federation of Analytical Chemistry and Spectroscopy Societies - Bioanalytical-Raman*. 2008.
29. Alimova, A., et al., *In vivo molecular evaluation of guinea pig skin incisions healing after surgical suture and laser tissue welding using Raman spectroscopy*. Journal of Photochemistry and Photobiology B-Biology, 2009. **96**(3): p. 178-183.
30. Hunt, C.R., et al., *Genomic instability and enhanced radiosensitivity in Hsp70.1- and Hsp70.3-deficient mice*. Mol Cell Biol, 2004. **24**(2): p. 899-911.
31. Robichaux-Viehoever, A., et al., *Characterization of Raman spectra measured in vivo for the detection of cervical dysplasia*. Appl Spectrosc, 2007. **61**(9): p. 986-93.
32. Frank, C.J., R.L. McCreery, and D.C. Redd, *Raman spectroscopy of normal and diseased human breast tissues*. Anal Chem, 1995. **67**(5): p. 777-83.
33. Frank, C.J., et al., *Characterization of human breast biopsy specimens with near-IR Raman spectroscopy*. Anal Chem, 1994. **66**(3): p. 319-26.
34. Beere, H.M., *Death versus survival: functional interaction between the apoptotic and stress-inducible heat shock protein pathways*. The Journal of Clinical Investigation, 2005. **115**(10): p. 2633-2639.
35. Morimoto, R.I., P.E. Kroeger, and J.J. Cotto, *The transcriptional regulation of heat shock genes: a plethora of heat shock factors and regulatory conditions*. Exs, 1996. **77**: p. 139-63.
36. Capon, A., et al., *Laser assisted skin closure (LASC) by using a 815-nm diode-laser system accelerates and improves wound healing*. Lasers Surg Med, 2001. **28**(2): p. 168-75.
37. Souil, E., et al., *Treatment with 815-nm diode laser induces long-lasting expression of 72-kDa heat shock protein in normal rat skin*. Br J Dermatol, 2001. **144**(2): p. 260-6.

CHAPTER III

FUTURE DIRECTIONS

For the first time, Raman spectra have been characterized as a function of both space and time for a healing incisional wound *in vivo*. The role of HSP70 was examined in both normal and laser preconditioned wound healing. Results from this study suggest that HSP70 plays an active role in normal wound healing. Moreover, the downstream tissue-level effects of HSP70 are augmented by laser preconditioning. Raman spectra identified differences in wound healing time course as a function of genetic expression and treatment response. Raman spectra peak ratios suggest that HSP70 increased protein conformational organization throughout the first postoperative week. Peak ratios also indicate HSP70 induced cellularity increases during inflammatory and early reepithelialization phases. Finally, the same peak ratios suggest that laser pretreatment extends the duration of HSP70 dependent increased cellularity. While the results justify continuing translation from a preconditioning to conditioning environment to augment healing of existing wounds as a function of HSP70 expression, they also suggest numerous avenues for the application of Raman Spectroscopy as a non-invasive, hand-held, quantitative, real-time, high-throughput, relatively inexpensive method of wound healing diagnosis.

Laser preconditioning has been established in animal models, mostly in mice, and its mechanisms are beginning to become clear. Preconditioning and its post-wound "conditioning" counterpart now require transition to more physiologically relevant animal models (rats then pigs) to secure future clinical relevance. Clinically, preconditioning is practically limited to elective surgeries and possible planned grafting applications, though the latter has not been established. However, conditioning (applying laser light after the wound has already been induced) would be most useful in impaired wound healing. Application of laser conditioning to

impaired wounds will require optimization and therefore some method of non-invasive in-situ feedback. Therefore both laser treatment and Raman spectroscopy will focus on wound models representing the highest clinical need. Development of Raman spectroscopy for classification and content quantification via convolution will be evaluated in diabetic and aged wound models of splinted excisions and ischemic flaps. The key to success in this study will be establishing a spectral characteristic of each of the phases of wound healing and how they change as a function of disease.

Raman spectroscopy was established in the most basic wound model, limiting interference due to changing light transport dynamics that will be seen in a large or impaired wound bed. Feasibility studies will be conducted to ensure sample size needs for future statistical power measures by quantifying machine variance and sample variance in normal rat excisional wounds. This data will also be used to ensure the validity and stability of fluorescence subtraction algorithms developed for cancer detection. These studies will require brief acquisition parameter optimization. Surgical materials will be analyzed for possible scaled background subtraction to prevent interference. This work is already under way and its results will allow for rapid transition to the rat wound model with laser conditioning when needed.

To ensure feasibility of transition of preconditioning to conditioning, an initial parametric optimization study will utilize incisional wounds in our HSP70–luciferase mouse model. The study will test two optimized protocols (constant temperature and constant irradiance) while evaluating several time points to determine to what extent post wound generation is the therapy protocol valid. In all mouse studies, HSP70 upregulation will be measured through Bioluminescence Imaging at several time points prior to and post treatment. Downstream effects will be evaluated with HSP70 immunohistochemistry and tensiometry at time points similar to those used for previous studies. Development of a protocol for excisional wounds will require

beam shaping or blocking as well as laser output scaling to achieve the same irradiances as in the parametric study. Excisional wounds will be evaluated using HSP70 immunohistochemistry and advanced histological scoring, made possible in this model due to large scale reepithelialization. With optimized data from murine excisions, a short parametric optimization will allow for transition to rat excision wounds. Without luciferase transgene, rat studies will depend on downstream effects of HSP70 measured by Raman spectroscopy and histology to confirm treatment efficacy. Results of these studies will be a starting point for ischemic flap and diabetic excision treatment in rats that will utilize Raman spectroscopy. Feasibility studies will provide optimization for real-time *in vivo* analysis for these studies.

Established treatments for healing wounds are mostly protocols to improve on older dressings, offloading, or debridement techniques. These types of advances are needed but focus on decreasing healing time by avoiding complications that retard wound healing, rather than actually accelerating the healing process. There are a limited number of successful topical gels containing growth factors though they remain largely experimental and very expensive. Contact-based heating methods that currently exist for other applications require clinically intractable, unacceptable risk or infection, pain and tissue damage that prevent use in this field. Wounds also tend to occur over bony processes, making controlled contact and precise conduction difficult. Laser thermal modulation treatments directly address these limitations by tuning wavelength and irradiance to achieve non-contact, controlled heating in time and space. In contrast to topical therapies, laser conditioning is relatively inexpensive and utilizes the body's endogenous response. This therapy has a potential to improve healing time and tissue quality, leading to a decrease in complications and reoccurrences.

Current wound healing diagnostics differ greatly between laboratory and clinical research, often cited as the source of great disparity in recent study results. Clinical methods are

comprised of photometric calculations of closure, subjective scoring rubrics, or invasive biopsies. Laboratory methods are more quantitative but destructive or very limited in scope. Tensiometry, a common laboratory method, provides biomechanical information about the healing wound at the expense of destroying the sample. Histology provides excellent information about structure and content, but requires sample removal, preparation and scoring by a team of experts. Raman spectroscopy directly addresses these limitations as a complementary modality for in-situ, non-invasive, quantitative measures of tissue-level properties. While Raman will not provide the precision of immunohistochemistry, it has the advantages of near-realtime collection and automated processing in a hand-held system. Raman spectroscopy has the potential to improve differential diagnosis in the clinic while providing a modality for testing new therapies that readily translates from the laboratory to the clinic.